Mitochondrial dysfunction induces dendritic loss via eIF2α phosphorylation

Taiichi Tsuyama, Asako Tsubouchi, Tadao Usui, Hiromi Imamura, and Tadashi Uemura

Graduate School of Biostudies, Kyoto University, Kyoto 606-8501, Japan

Mitochondria are key contributors to the etiology of diseases associated with neuromuscular defects or neurodegeneration. How changes in cellular metabolism specifically impact neuronal intracellular processes and cause neuropathological events is still unclear. We here dissect the molecular mechanism by which mitochondrial dysfunction induced by Prel aberrant function mediates selective dendritic loss in *Drosophila melanogaster* class IV dendritic arborization neurons. Using in vivo ATP imaging, we found that neuronal cellular ATP levels during development are not correlated with the progression of dendritic loss. We searched for mitochondrial stress signaling pathways that induce dendritic loss and found that mitochondrial dysfunction is associated with increased eIF2α phosphorylation, which is sufficient to induce dendritic pathology in class IV arborization neurons. We also observed that eIF2α phosphorylation mediates dendritic loss when mitochondrial dysfunction results from other genetic perturbations. Furthermore, mitochondrial dysfunction induces translation repression in class IV neurons in an eIF2α phosphorylation-dependent manner, suggesting that differential translation attenuation among neuron subtypes is a determinant of preferential vulnerability.

Introduction

Mitochondria are key contributors to the etiology of a wide array of diseases with neuromuscular defects or neurodegeneration (DiMauro and Schon, 2008; Nunnari and Suomalainen, 2012). Mutations within genes encoding proteins that are essential for oxidative phosphorylation (OXPHOS) cause primary mitochondrial diseases with severe neuronal deficits (Koopman et al., 2012). Mitochondrial dysfunction is also closely associated with neurodegenerative disorders, including Parkinson's disease (PD; Itoh et al., 2013; Haelterman et al., 2014). Tissues from patients and model animals show a range of mitochondrial dysfunction–related features, including mitochondrial fragmentation, mislocalization of mitochondria, and loss of respiratory enzyme activities (Wallace and Fan, 2009; Greaves et al., 2012). Mitochondrial dysfunction in these diseases and their models results in a variety of neuropathological events, including neuronal loss, axonal degeneration, and dendritic pathology (Patt et al., 1991; Cheng et al., 2010). Although it is commonly accepted that high energy demands in neurons render the nervous system vulnerable to mitochondrial dysfunction, how the disturbance in cellular energy supply impacts cellular energy requiring processes in neurons and causes each neuropathological event is unclear (Pathak et al., 2013).

Because mitochondria play a pivotal role in energetic metabolism, mitochondrial malfunction often causes changes in energy-related indicators (such as [ATP], [ATP/AMP], and [NAD^+/NAD]; Nunnari and Suomalainen, 2012). The changes can act as cellular signals that directly affect signaling components, including the ATP-dependent potassium channel, the proteasome, AMPK, and sirtuins (Ying, 2008; Huang et al., 2010; Hardie et al., 2012; Tanaka et al., 2014). Consequently, these signaling events will alter diverse cellular activities, such as translocation of ions across membranes and synthesis and degradation of proteins, which may contribute to the etiology of neuronal diseases. However, the relationships between these indicators and neuronal phenotypes are still unclear.

Another major conundrum in the field of mitochondria-related diseases is how mitochondrial dysfunction leads to cellular subtype-specific pathologies of the diseases. Differential vulnerabilities in neuronal subpopulations are common in both mitochondrial DNA mutation–linked mitochondrial diseases and disorders caused by nuclear DNA mutations (Zhou et al., 1997; Rossignol et al., 2003; Haddad and Nakamura, 2015). Although several mechanisms of neuronal differential sensitivities in mitochondria-related disease have been proposed, our understanding is still incomplete (Dubinsky, 2009; Haddad and Nakamura, 2015).

These unsolved problems could stem from multiple causes, including technical limitations and the complexity of

Correspondence to Tadashi Uemura: tauemura@lif.kyoto-u.ac.jp

A. Tsubouchi's present address is Institute of Molecular and Cellular Biosciences, The University of Tokyo, Bunkyo-ku, Tokyo 113-0032, Japan.

Abbreviations used: 2-DG, 2-deoxyglucose; AEL, after egg laying; AM, antimycin; ANOVA, Analysis of variance; CHX, cycloheximide; da, dendritic arborization; FRET, Förster resonance energy transfer; KD, knockdown; MARCM, mosaic analysis with a repressible cell marker; O/E, overexpression; OXPHOS, oxidative phosphorylation; PC, photoconversion; PD, Parkinson's disease; ROI, region of interest; UPR, unfolded protein response.

The Rockefeller University Press $30.00
J. Cell Biol. Vol. 216 No. 3 815–834
https://doi.org/10.1083/jcb.201604065

mitochondria-derived signaling. Widely used methods to determine metabolite levels have provided insufficient spatial and temporal resolution to investigate neurons in detail, limiting our understanding of how altered bioenergetic metabolism leads to pathogenesis (Pathak et al., 2013). This technical limitation is beginning to be overcome, however. Recently introduced genetically encodable biosensors for metabolites have improved our understanding of dynamic energy metabolism in neurons at single-cell resolution (Surin et al., 2013; Connolly et al., 2014; San Martín et al., 2014; Toloe et al., 2014; Hasel et al., 2015; Pathak et al., 2015).

In addition, the complexity of mitochondrial stress signals continues to challenge our understanding of the molecular etiology (Raimundo, 2014; Monaghan and Whitmarsh, 2015). Because mitochondrial lesions can lead to the decline of various mitochondrial functions, diverse signaling pathways that sense mitochondrial status and transmit information to the rest of the cells have evolved for cellular adaptation and mitochondrial quality control. Sustained activation of these signals, including the ROS-AMPK-E2F1 and HIF1 pathways, has been proposed to contribute to the etiology of mitochondria-related neuronal disorders (Raimundo, 2014; Cagin et al., 2015). Again, despite these important clues, our understanding of how signals from dysfunctional mitochondria contribute to pathogenesis is still incomplete.

Drosophila melanogaster dendritic arborization (da) neurons are a group of peripheral sensory neurons that develop elaborate and stereotyped dendritic arbors. da neurons are classified as class I to IV with regard to their complexity and other characteristics of their dendritic arbors (Grueber et al., 2002; Jan and Jan, 2010). For example, class I neurons develop comb-like and short dendritic processes, and class IV neurons extend the most extensively branched and longest dendritic trees among the four classes. We previously reported the identification of *prel*, which is required for proper dendritic patterning of class IV neurons (Tsubouchi et al., 2009). *prel/UPS1* encodes a mitochondrial protein that facilitates transfer of phosphatidic acid between the inner and outer membrane (Tamura et al., 2009; Tatsuta et al., 2014). Both loss of function and overexpression (O/E) of *prel* induced mitochondrial dysfunction in various cell types (Tsubouchi et al., 2009). Knockdown (KD) of *prel* in *Drosophila* hemocytic S2 cells leads to reduced mitochondrial membrane potential, decreased enzymatic activity of respiratory complex IV, and reduced cellular ATP. O/E of Prel also reduces ATP levels in S2 cells and fly brains. These bioenergetic defects could be explained by impaired biosynthesis of functionally important lipids in mitochondria (Ren et al., 2014). Notably, loss of function and O/E of *prel* induced more severe dendritic loss in class IV neurons than in other neuronal classes. Thus, da neurons provide a unique model system to study mechanisms underlying dendritic pathology and differential fragility among neuronal classes faced with mitochondrial defects. Although proper dendritic shape is critical for functional connectivity of nervous systems, molecular mechanisms of dendritic pathology followed by mitochondrial dysfunction is still poorly understood.

In this study, we investigated the molecular mechanisms of subtype-selective dendritic loss induced by mitochondrial dysfunction in da neurons. We examined the progression of dendritic morphological development together with in vivo imaging of relative cellular ATP levels in neurons. In genetic models of mitochondrial dysfunction, we found that neuronal ATP levels during development were not correlated with the progression of dendritic loss. We then searched for signaling pathways that mediate mitochondrial stress signals and induce dendritic loss and found that eIF2α, which promotes general protein translational initiation, is a mediator of the dendritic pathogenesis. We also found that differential translational attenuation among the neuron classes could be a key determinant of selective vulnerability to mitochondrial dysfunction.

Results

Aberrant *prel* function induces dendritic regression of *Drosophila* peripheral sensory da neurons during larval development

prel/ups1p encodes a mitochondrial protein, and its O/E and loss of function results in mitochondrial OXPHOS impairment in various cell types (Tsubouchi et al., 2009). As we reported previously, O/E and loss of function of *prel* induce fragmentation of mitochondria in the cell body and the striking shortening of dendritic arbors of class IV ddaC (dorsal dendrite arborization neuron C) neurons in mature larvae (Fig. 1, A–C; Tsubouchi et al., 2009). Mitochondrial fragmentation is closely associated with mitochondrial dysfunction (Itoh et al., 2013). Despite similar fragmented mitochondrial morphologies in the *prel* mutant or O/E neurons, dendritic arbors of class I ddaE neurons and class III ddaA neurons are relatively resistant to altered *prel* function compared with those of class IV neurons (Fig. 1, D–I; and Fig. S1, A–F), as previously described. Hereafter, we refer to ddaC, ddaE, and ddaA neurons as class IV, I, and III neurons, respectively.

To better characterize the dendritic patterning defects induced by Prel O/E, we investigated the development of dendritic arbors of class IV neurons during larval development, specifically at 22–26 h after egg laying (AEL; the early first-instar larval stage, designated as early L1 hereafter), 46–50 h (designated as early L2), and the wandering third-instar stage (late L3). Dendritic patterning was not affected by Prel O/E at early L1, but dendritic arbors were strikingly shortened at early L2 and late L3 (Fig. 1, J–L′). Our time-lapse analysis showed that 42% of dendritic endings of wild-type class IV neurons at early L2 were eliminated or shortened after 24 h (Fig. 1 M); in contrast, 70% of dendritic endings of Prel-overexpressing class IV neurons were regressed after 24 h (Fig. 1, N and O). These results imply that the dendritic loss induced by Prel O/E was caused, at least in part, by destabilizing the dendritic terminals.

ATeam1.03NL is sensitive enough to detect reductions in ATP levels in class IV neurons

Next, we focused on ATP metabolism in da neurons. ATP metabolism was of particular interest for dendrite pathogenesis in our model because expansive dendritic arbors of class IV neurons may increase their membrane surface and result in higher ATP demands for energetically expensive processes associated with the cell membrane, such as transport of various ions across the cell membrane and membrane phospholipid metabolism (Purdon and Rapoport, 2007; Howarth et al., 2012). Indeed, previous transcriptomic analysis and our gene expression analysis indicated that class IV neurons express genes related to OXP HOS at higher levels than other classes (Iyer et al., 2013; see

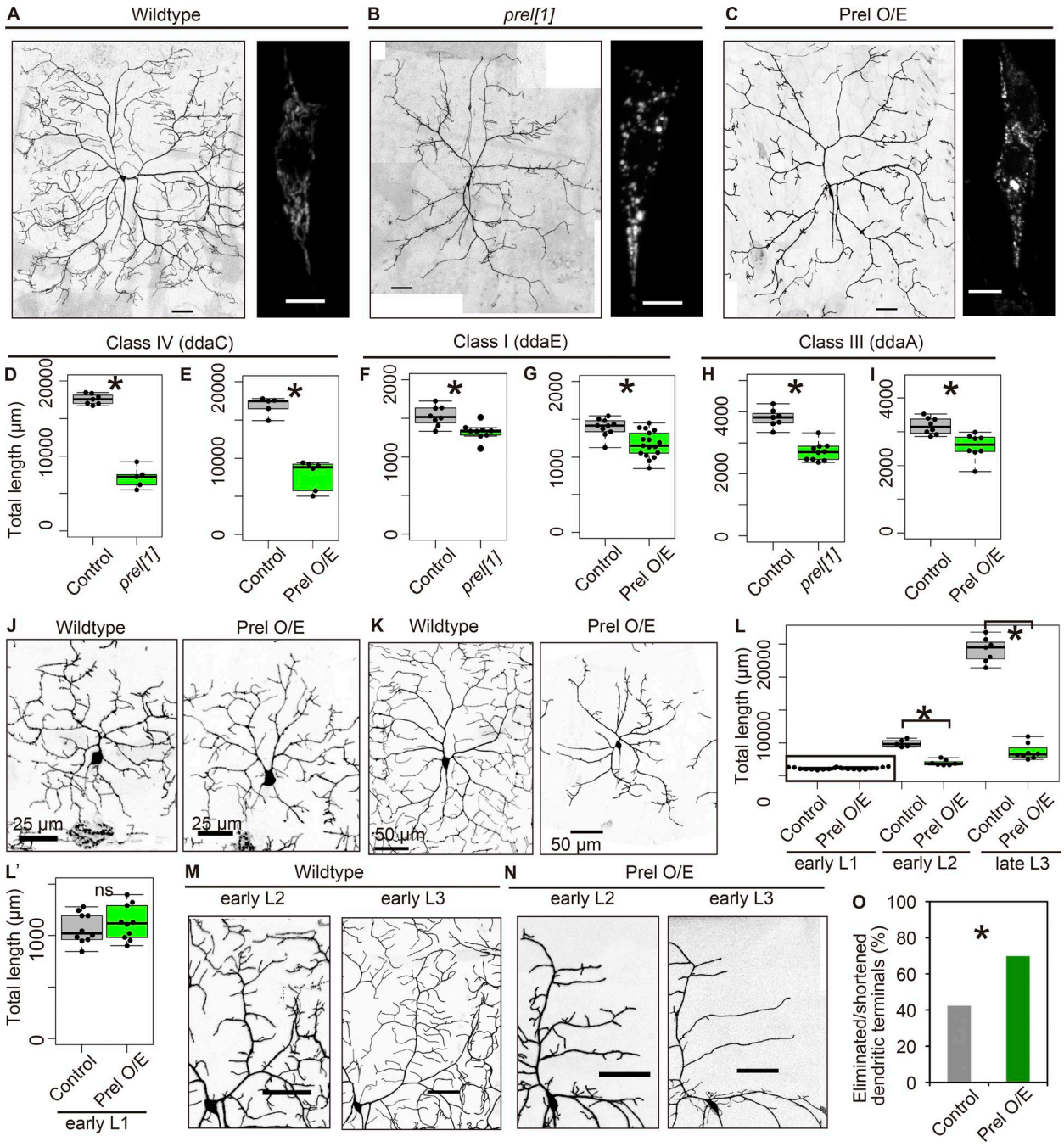

Figure 1. **Dendritic arbors of class IV neurons show vulnerability to altered *prel* function.** (A–C) Representative dendritic and somal mitochondrial morphologies of wild-type (A), *prel[1]* mutant (B), and Prel-overexpressing (O/E; C) class IV neurons. Dendritic arbors and mitochondria were visualized with membrane-bound GFP and mitoGFP, respectively. Bars: (dendrite images) 50 μm; (mitochondrial images) 5 μm. (D–I) Quantification of the total dendritic length of *prel[1]* mutant (D, F, and H) and Prel-overexpressing (E, G, and I) da neurons. Total length values of each neuron were plotted, and boxplots represent median and interquartile ranges. Class IV neurons (D and E) showed more severe dendritic losses than class I (F and G) and class III (H and I) neurons. (J–L) Developmental changes in the total length of class IV neuron dendrites. Representative images of dendritic arbors of class IV neurons at early L1 (22–26 h AEL; J) and at early L2 (46–50 h AEL; K). Prel was expressed by using a pan da neuronal Gal4 driver *Gal4*$^{109(2)80}$, which expresses from early in embryonic development onward (Gao et al., 1999). Quantification of the total dendritic length of wild-type and Prel-overexpressing class IV neurons throughout larval development (L and L'). Plots of early L1 larvae (a black box in L) are magnified in L' for clarity. (M–O) Time-lapse analysis of larval dendritic development. Representative images of wild-type (M) and Prel-overexpressing (N) Class IV neurons. Quantification of regression of preexisting terminals (O) shows decreased stability of terminals of class IV arbors overexpressing Prel (n = 860 terminals from four neurons for control and 701 terminals from six neurons for Prel O/E). Bars, 50 μm. *, $P < 0.05$; ns, not significant. The statistical tests used, exact p-values, 95% confidence intervals, and sample sizes in this and subsequent figures are summarized in Table S1, and genotypes are summarized in Table S2.

Materials and methods), suggesting higher energy demand in class IV neurons (Wong-Riley, 2012).

We determined the relative ATP content in da neurons in vivo by taking advantage of Förster resonance energy transfer (FRET)–based ATP biosensors, ATeams (Imamura et al., 2009). FRET efficiencies of ATeams increase upon ATP binding to the linker peptide. ATeam1.03NL (AT[NL]) is optimized for use at relatively lower temperatures (20–30°C; Tsuyama et al., 2013) and is predicted to detect changes in ATP levels in the range of 0.5 to 4 mM at 25°C (Fig. S2 A). Importantly, it is commonly reported that neuronal ATP concentrations are in this range (Erecińska and Silver, 1989; Rangaraju et al., 2014; Pathak et al., 2015). Prel O/E in S2 cells decreased the FRET signal (the FRET/CFP emission ratio) of AT[NL] compared with the control (Fig. 2 A), consistent with our previous result obtained with a luciferase-based assay (Tsubouchi et al., 2009). In contrast, Prel O/E did not affect the FRET signal of ATeam1.03RKRK (AT[RK]; Fig. 2 A), which does not bind ATP (Imamura et al., 2009), demonstrating that the decrease in the AT[NL] signal is ATP-binding dependent. These results indicate that AT[NL] is sufficiently sensitive to detect decreases in ATP levels that could be induced by chronic mitochondrial dysfunction in *Drosophila* cells.

To monitor changes in FRET signals of da neurons in response to reductions in ATP levels, we performed time-lapse imaging of da neurons treated with antimycin (AM), an inhibitor of the respiratory complex III, and/or 2-deoxyglucose (2-DG), an inhibitor of glycolysis, in dissected preparations. The basal FRET signal of AT[NL] in the cell body of class IV neurons at late L3 was markedly higher than that of AT[RK] (Fig. 2 B). The basal AT[NL] signal was stable over 1 h in the fillet preparation (Fig. S2 B). When OXPHOS was blocked by bath application of AM, the initial high signal of AT[NL] in class IV neurons quickly and strikingly dropped to a level comparable to that of AT[RK] (Fig. 2, B and C), indicating that the acute OXPHOS inhibition dramatically reduced cellular ATP. Importantly, the apparent reductions took place within a few minutes (Figs. 2 B and S2 B), confirming the notion that AT[NL] is highly sensitive to ATP changes in class IV neurons. The 2-DG addition resulted in a small drop in the AT[NL] signal (Fig. 2 C), suggesting that the ATP supply from glycolysis is less than ATP derived from OXPHOS in wild-type class IV neurons. Rapid reductions of ATP levels upon OXPHOS inhibition were also observed in other class IV neurons (i.e., v′ada and vdaB neurons; see Fig. S2 C). In contrast to class IV neurons, inhibition of ATP production with AM plus 2-DG in class I and III neurons caused delayed drops in the AT[NL] signal with lag periods (~10–15 min) preceding drops in the signals. These lag periods may be explained by several possibilities, including the saturated FRET efficiency of AT[NL] in class I and III neurons (Fig. S2 D and its legend).

ATP concentrations are largely preserved in Prel-overexpressing class IV neurons at larval stages when severe dendritic defects are observed

In light of the fact that sudden inhibition of OXPHOS leads to a precipitous decrease in ATP levels, we asked whether altered *prel* function also affects ATP levels in class IV neurons. To address this question, we measured the FRET signals in the soma during larval development and compared the signals between control and Prel O/E at distinct stages (Fig. 2, D, E, and G) or between control and *prel[1]* mutant neurons (Fig. 2 F). (We did not perform direct comparisons of FRET signals between different developmental stages. See the explanation in Materials and methods.) In early L1, Prel O/E lowered the FRET signal of AT[NL] (Fig. 2 D), but it did not affect that of AT[RK] (Fig. 2 E), indicating a decrease in ATP levels by Prel O/E. As dendritic arbors of neurons with Prel O/E at early L1 were not morphologically different from controls (Fig. 1, J, L, and L′), dendritic growth of class IV neurons at this early larval stage appeared to be relatively resistant to mitochondrial dysfunction and subsequent ATP depletion. Similar reductions in the FRET signals were observed in class I and III neurons (Fig. S2 E). At early L2 and early L3, Prel O/E resulted in increased FRET signals of AT[NL] (Fig. 2 D). At early L3, it also elevated the AT[RK] FRET signal (Fig. 2 E), suggesting the increase was at least partially ATP-concentration independent. At late L3, neither Prel O/E nor loss of function of *prel* led to significant changes in the FRET signal (Fig. 2, D and F). Similarly, no significant change in the AT[NL] FRET signal was apparent in dendritic arbors of Prel-overexpressing class IV neurons at early L3 (Fig. 2 G). These results suggest that class IV neurons with altered *prel* function preserved physiologically relevant ATP levels at least from early L2 stages onward, even when severe dendritic defects were observed.

Enhanced glucose utilization and reduced ATP consumption in class IV neurons contribute to maintenance of ATP levels

In later larval stages, the ATP conservation in class IV neurons that exhibited severe mitochondrial fragmentation could be explained by compensational energy supply from sources other than mitochondria and/or reduced energy consumption used for cellular activities. Next, we addressed these possibilities. Glycolysis is able to produce the bulk of ATP, and it is frequently up-regulated in neurons with OXPHOS impairment (Malthankar-Phatak et al., 2008; Misko et al., 2012). To examine whether a dependency on glycolysis for ATP production was increased or not, we investigated the effects of inhibitors of ATP production pathways on the AT[NL] FRET signal. 2-DG treatment decreased the signals in both control and Prel-overexpressing neurons of the three classes tested, except for the control class I neurons (Fig. 3 A). Moreover, the decreases in the signals of Prel O/E class I, III, and IV neurons were greater than those in control neurons. In contrast, the decrease of the FRET signals induced by mitochondrial inhibitors was slower in *prel* O/E and loss-of-function class IV neurons than in control neurons (Fig. 3, B and C; and Fig. S3, A–C). These results imply that da neurons with altered *prel* function are more dependent on glycolysis for ATP production. We also assessed glucose uptake in class IV neurons using a fluorescent analogue of glucose (2-NBDG; Itoh et al., 2004). Although quantitative measurement of 2-NBDG uptake in class IV neurons was difficult because of strong signals of 2-NBDG incorporated by surrounding tissues (i.e., the epidermis and body wall muscle), distributions of signals were significantly different between the control and Prel O/E genotypes. In the control, the fluorescent signal of 2-NBDG was detected around class IV neuronal soma, which presumably represents uptake by surrounding glial cells (Fig. 3 D and Fig. S1, G–I). In contrast, 2-NBDG was efficiently taken up by neuronal cell bodies of Prel O/E class IV neurons (Fig. 3 D, arrowheads), suggesting glucose utilization was up-regulated. These observations, along with our previous biochemical evidence for

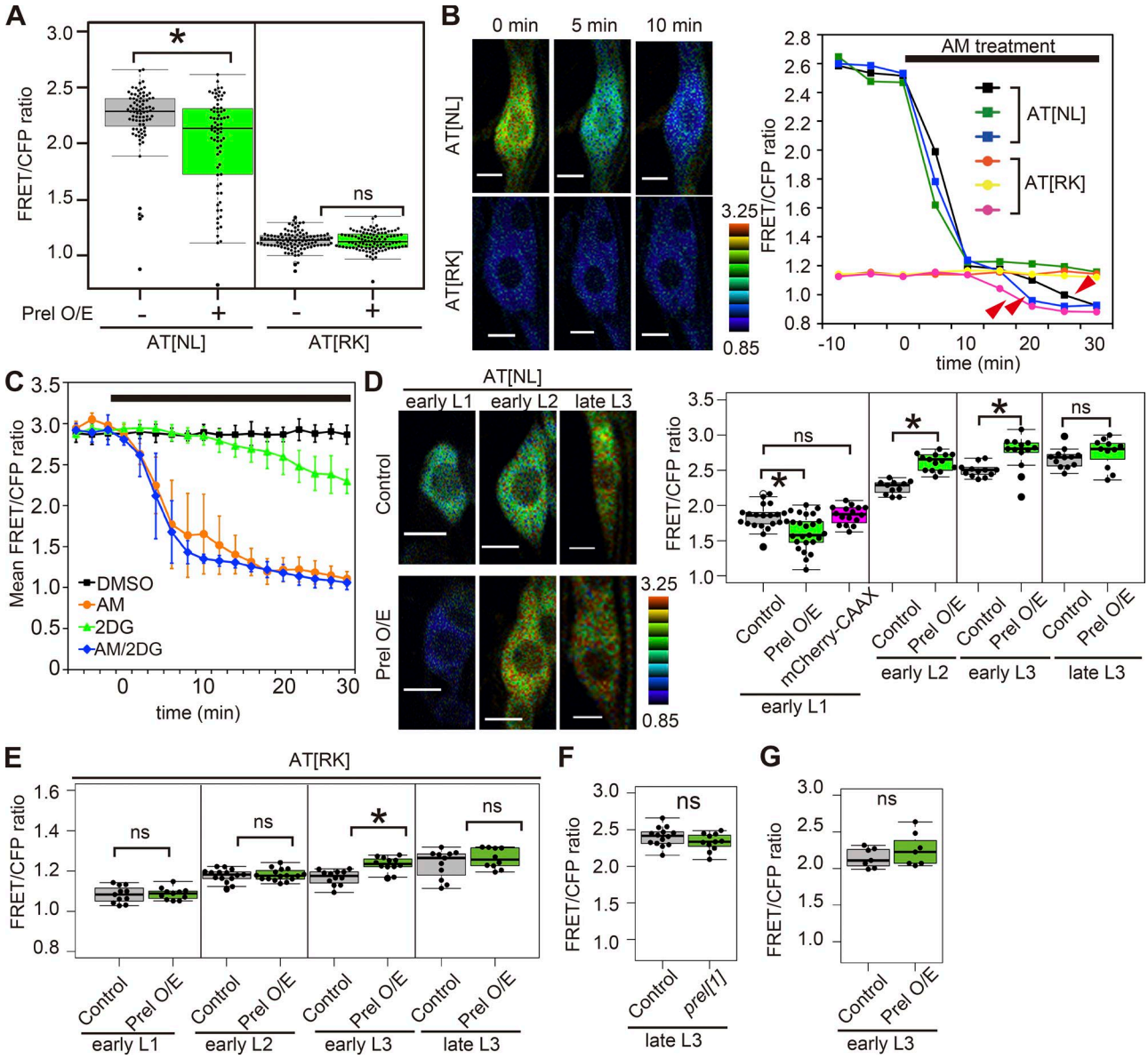

Figure 2. **The FRET signal of AT[NL] reports ATP levels in class IV neurons.** (A) Prel O/E in S2 cells decreased the FRET signal (FRET/CFP emission ratio) of AT[NL], but not that of AT[RK]. Prel plus either AT[NL] or AT[RK] were transiently coexpressed in S2 cells using *actin-Gal4*. Plots indicate the FRET signal values of individual cells. Similar results were obtained in three or more independent experiments. (B and C) Real-time imaging of ATeams in class IV neurons of dissected larvae. Representative pseudocolored images of the FRET signals of class IV neuronal soma expressing AT[NL] or AT[RK] (B, left) in the presence of 100 µM antimycin (AM), an inhibitor of the respiratory complex III. Representative plots of the signal values in individual neurons (B, right). A thick black line indicates the duration of AM treatment. Arrowheads in B (right) indicate ATP-independent drops of the signals of ATeams (see also Materials and methods) in class IV neurons treated with AM. (C) Changes in mean signal values of AT[NL] in class IV neurons treated with inhibitors of glycolysis and/or OXPHOS. AM and 2-deoxyglucose (2-DG), an inhibitor of glycolysis, were used at a concentration of 50 µM and 50 mM, respectively. Values are mean ± SD. (D and E) FRET imaging of class IV neurons expressing ATeams plus Prel driven by *Gal4*$^{109(2)80}$ in whole live larvae. Pseudocolored images (D, left) and quantification (D, right) of the FRET signals of AT[NL]. Plots indicate the FRET signal values in each neuron. We coexpressed the *mCherry-CAAX* transgene as a control for UAS copy-number dependence and did not detect significant changes in the signal. (E) Quantification of the signals of AT[RK] in class IV neurons over larval development. (F) Quantification of the FRET signals of AT[NL] in the cell body of wild-type and *prel[1]* mutant class IV MARCM clones at late L3. (G) Quantification of the FRET signals of AT[NL] at the distal parts of dendritic arbors (>100 µm distant from the cell body along dendrites) of class IV neurons. Prel and AT[NL] were expressed with a class IV–specific *ppk-Gal4* driver. Bars, 5 µm. *, $P < 0.05$; ns, not significant.

mitochondrial dysfunction in S2 cells with altered *prel* function (Tsubouchi et al., 2009), imply the possibility that Prel O/E causes mitochondrial dysfunction in da neurons, resulting in compensational up-regulation of glycolysis.

Cellular ATP levels are determined not only by the ATP synthesis rate but also by the balance between supply and demand of ATP (Brand, 1997; Hofmeyr, 2008). We treated class IV neurons with AM plus 2-DG to block the major ATP-producing pathways and observed the time course of the decrease in the FRET signal as a surrogate for the ATP consumption rate (Fig. 3 E). Simultaneous inhibition of OXPHOS and glycolysis rapidly decreased the FRET signal in wild-type class IV neurons (Figs. 2 C and 3 E), whereas the rate of signal decline in Prel-overexpressing class IV neurons was significantly slower (Figs. 3 E and S3 D). These results argue that Prel-overexpressing class IV neurons consume less ATP than

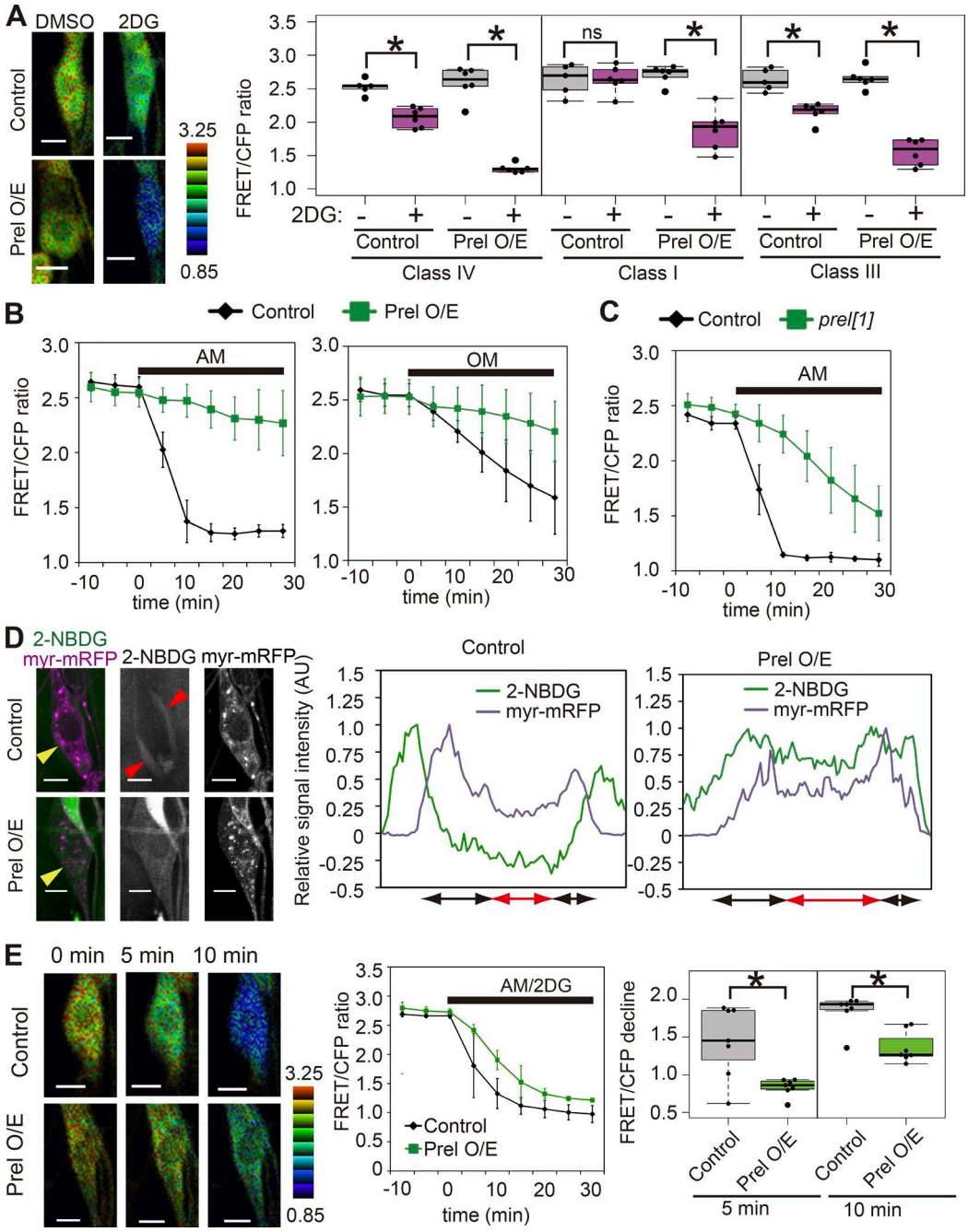

Figure 3. **Prel-overexpressing class IV neurons preserve ATP levels by alterations in energy supply and demand.** (A) FRET imaging of Class IV neurons expressing AT[NL] plus Prel in the absence or presence of 2DG (50 mM, 30 min). Pseudocolored images (A, left) and quantification (A, right) of the FRET signals of AT[NL]. (B and C) Time courses of changes in the FRET signals of AT[NL] in class IV neurons with Prel O/E (B) or loss of function of *prel* (C) in the absence or presence of AM (50 µM; $n = 5$ for each genotype) or oligomycin (OM; an inhibitor of ATP synthase; 100 µM; $n = 7$ for each genotype). Values are mean ± SD (D) 2-NBDG imaging of class IV neurons of dissected larvae. Representative images of 2-NBDG signals around the cell bodies of wild-type (top row) and Prel O/E (second row) class IV neurons (left). Yellow arrowheads indicate cell bodies of class IV neurons, and red arrowheads indicate the accumulation of 2-NBDG in a wild-type larvae. To clearly reveal features, these images were nonlinearly adjusted. We observed six class IV neurons from six larvae for each genotype, and similar patterns of 2-NBDG fluorescent signals were observed. Representative two-dimensional graphs of fluorescent signals along a line crossing the cell body of control and Prel-overexpressing class IV neurons (D, right). Quantification is based on images that are not nonlinearly adjusted. Each x axis represents distance along the respective lines. Black and red double-headed arrows under the graphs indicate the regions of the cytoplasm and the nucleus, respectively. Fluorescent peaks of the control were not located within class IV neurons (visualized by myr-mRFP) but surrounded the class IV soma. These signals may represent 2-NBDG captured by glial cells that wrap around cell bodies and axons of da neurons (Yamamoto et al., 2006; see also Fig. S1, G–I). Consistent with this notion, glial cells in *Drosophila* partially degrade sugars and provide alanine and lactate as intermediate metabolites for neurons (Schirmeier et al., 2015). (E) Real-time FRET imaging revealed that Prel O/E reduced the rate of ATP consumption of class IV neurons. Representative pseudocolored images of the FRET signals of soma expressing AT[NL] in control (top row) and Prel-overexpressing (second row) class IV neurons in the presence of 100 µM AM and 50 mM 2-DG (E, left). Changes in mean values of the AT[NL] signal (E, middle). Error bars represent SD. Plots of the signal decline of each neuron (E, right). Bars, 5 µm. *, $P < 0.05$; ns, not significant.

wild-type class IV neurons. Thus, class IV neurons with chronic mitochondrial dysfunction caused by Prel O/E may compensate for reduced energy production by both up-regulating glucose import and reducing ATP consumption.

eIF2α phosphorylation mediates the dendritic loss induced by Prel O/E

In a variety of model systems used to study energy stresses, the compensatory activation of glycolysis is controlled by energy stress pathways (Weisová et al., 2009; Requejo-Aguilar et al., 2014). Concomitantly, such stress signaling pathways inhibit many energy-requiring cellular processes (Storey and Storey, 2007; Hardie et al., 2012). We hypothesized that chronic mitochondrial malfunction leads to induction of stress signaling, which alters growth and/or stability of class IV dendritic arbors, resulting in dendritic loss. To test this hypothesis, we examined whether the dendritic patterning defect induced by Prel O/E was restored or not by coexpressing modulators of mitochondrial stress pathways in class IV neurons (Owusu-Ansah et al., 2008; Baker et al., 2012).

We tested several known mitochondrial stress pathways and found that many of the candidate genes failed to mitigate, or very weakly mitigated, the dendritic loss (Fig. 4 A). We did find an interesting exception, however; the gene *dPPP1R15*, which is functionally related to eIF2α, showed a significant genetic interaction with Prel O/E (Fig. 4, B–E). eIF2α is the α subunit of eIF2, and its active form promotes general protein translational initiation by stabilizing the 43S preinitiation complex (Wek et al., 2006). Upon diverse environmental stresses, including mitochondrial dysfunction, eIF2α is phosphorylated at a conserved serine residue by eIF2α kinases, and this phosphorylation blocks general translation in the cytoplasm (Wek et al., 2006; Baker et al., 2012). PPP1R15 family proteins are regulatory subunits of protein phosphatase complexes and enhance dephosphorylation of several interacting proteins, including eIF2α (Bollen et al., 2010; Malzer et al., 2013). We confirmed that ubiquitous expression of dPPP1R15 at midlarval stages strongly decreased basal phosphorylation of eIF2α compared with controls (Fig. 4 B).

Coexpression of dPPP1R15 with Prel in class IV neurons potently alleviated the dendritic loss in approximately two-thirds (11 out of 17) of the neurons that we observed at late L3 (Fig. 4, C and E, left); curiously, however, other neurons (6 out of 17) seemed to suffer from even severer dendritic loss than neurons overexpressing Prel alone (Fig. 4, C and E, right). We speculate that their dendritic arbors were often damaged and subsequently engulfed by the phagocytic epidermal cells (Han et al., 2014), which may partly contribute to the more severe phenotype (Fig. S4 A). The dendritic phenotypes of *prel* mutant neurons were also partially rescued by dPPP1R15 O/E (Fig. 4 F). In the wild-type background, dPPP1R15 O/E by itself did not significantly change dendritic arbor morphology (Fig. S4 B). In the Prel plus dPPP1R15–overexpressing neurons, mitochondria were just as highly fragmented as in Prel-overexpressing neurons, suggesting that mitochondrial function was not restored by dPPP1R15 coexpression (Fig. S4 D).

To further investigate the contribution of eIF2α phosphorylation to the dendrite phenotype, we explored whether two *Drosophila* eIF2α kinases, *Perk* and *Gcn2* (Pomar et al., 2003), are required for the dendritic loss by Prel O/E. The dendritic phenotype was markedly ameliorated by KD of *Perk*, but not *Gcn2* (Fig. 4 G); moreover, KD of *Perk* alone in the wild-type class IV neurons did not affect their dendritic length (Fig. S4 C), implying that Perk-mediated eIF2α phosphorylation contributes to the dendritic loss induced by mitochondrial malfunction. Perk-overexpressing class IV neurons developed shortened and less branched dendritic patterns, similar to Prel-overexpressing neurons (Fig. 4 H), suggesting that a forced increase in eIF2α phosphorylation is sufficient for dendritic loss.

Translational regulators S6 kinase/S6k and 4E-BP/Thor have been reported to genetically interact with *Drosophila* PD models (Tain et al., 2009; Liu and Lu, 2010). Neither was positive for the interaction test under the genetic conditions that we used (Fig. 4, C and G). Therefore, the genetic interaction between Prel O/E and the presumed enhancement of translational activity by eIF2α dephosphorylation was specific, as far as we tested.

Prel O/E induces translational repression in class IV neurons in an eIF2α phosphorylation–dependent manner

Next, we examined whether mitochondrial dysfunction is able to increase the relative amount of phosphorylated eIF2α (P-eIF2α) and repress translation in vitro and in vivo. We treated the *Drosophila* culture cell lines S2 and Dm BG2-c2 that is an immortalized cell line derived from the *Drosophila* larval central nervous system (Ui-Tei et al., 1994), with various mitochondrial inhibitors (AM, OM, and CCCP [carbonyl cyanide 3-chlorophenylhydrazone], an uncoupler of the mitochondrial proton gradient; Fig. S4 E). Although P-eIF2α in S2 cells treated with AM was decreased, P-eIF2α in Dm BG2-c2 cells was increased by mitochondrial inhibitors. We also found that Prel O/E coincided with increased P-eIF2α in adult heads when compared with controls (Fig. 5 A), and the increase was partially suppressed by KD of *Perk* (Fig. 5 B). These results suggest that mitochondrial dysfunction is capable of inducing eIF2α phosphorylation in *Drosophila* cells.

To assess the effect of Prel and/or dPPP1R15 O/E on protein synthesis, we monitored de novo protein synthesis in da neurons at single-cell resolution with Kaede, a photoconvertible fluorescent protein. Kaede undergoes an irreversible peptide cleavage–mediated green-to-red photoconversion (PC) upon UV irradiation (Mizuno et al., 2003). This irreversible conversion of preexisting Kaede enabled us to measure de novo Kaede synthesis after the PC by monitoring recovery of green fluorescence (Leung and Holt, 2008; Chen et al., 2012). In wild-type larvae at the early L3 stage, striking recovery of green fluorescence was detected 6 h after UV irradiation, and this recovery was completely blocked by feeding the larvae cycloheximide (CHX), an inhibitor of protein synthesis (Fig. 5 C).

In class IV neurons, Prel O/E significantly impeded fluorescence recovery, and dPPP1R15 coexpression reversed this blockage (Fig. 5, D–G and H, left), consistent with the idea that enhanced eIF2α phosphorylation by Prel O/E repressed translation and that dPPP1R15 counteracted this effect. On the other hand, in class I and III neurons, the repressive effects of Prel O/E on fluorescence recovery were smaller than that of class IV neurons and did not reach the threshold we adopted for statistical significance (Fig. 5 H). We consider that the decrease in the fluorescent intensity was primarily caused by lowered protein synthesis and that the contributions of protein degradation and the transcriptional control would be less likely. This is because the decrease in the intensity was ameliorated by dPPP1R15 O/E (Fig. 5 H, left). Furthermore, we imaged signals of Kaede that had been photoconverted and observed no obvious differences in the intensity between control and Prel O/E just after the PC

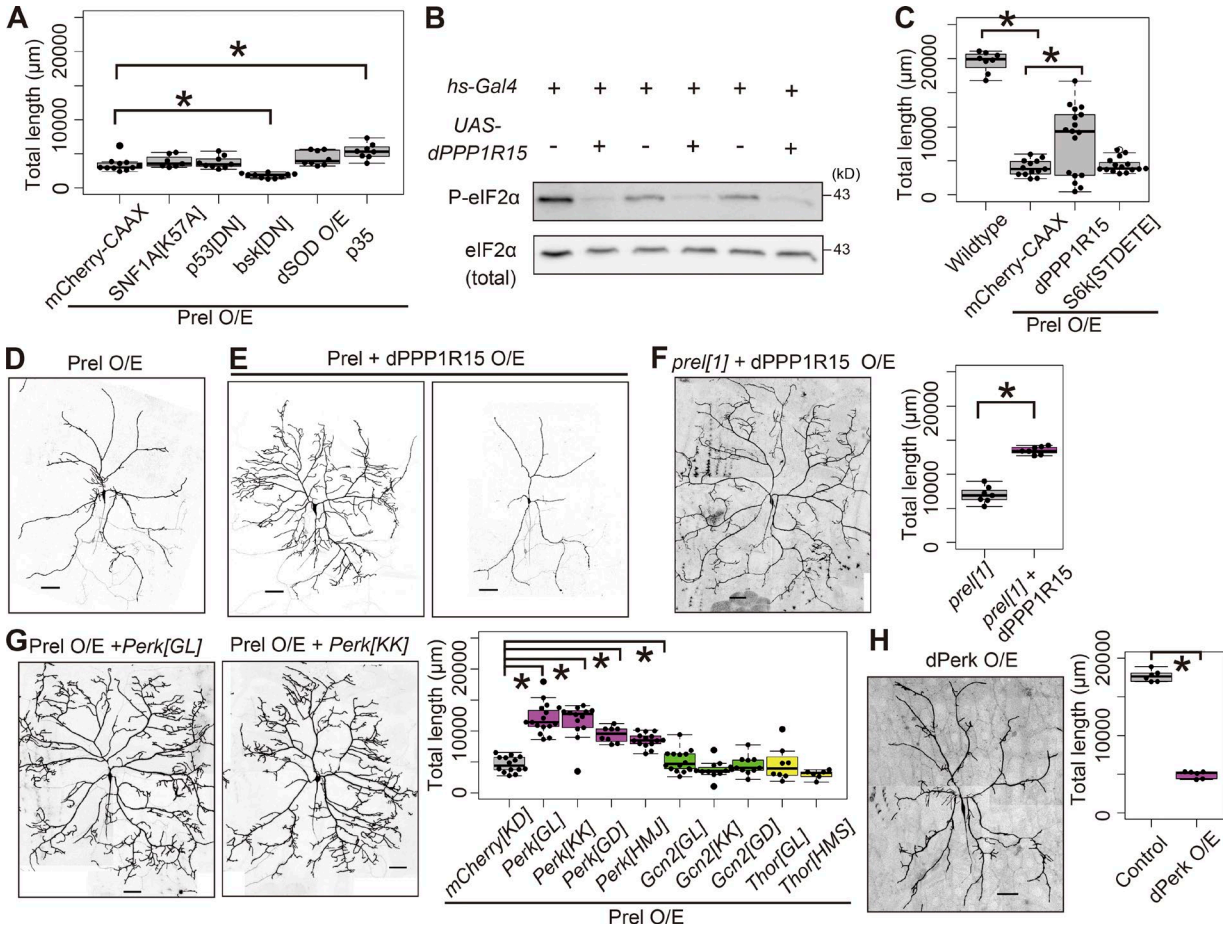

Figure 4. **Promotion of eIF2α dephosphorylation prevents the dendritic loss induced by prel O/E.** (A) The effect of repression of candidate pathways of mitochondria-derived stress signaling on the dendritic loss induced by Prel O/E in class IV neurons. bsk[DN], a dominant-negative form of JNK; p53[DN], a dominant-negative form of p53; SNF1A[K57A], a kinase inactive form of AMPK catalytic subunit (Adachi-Yamada et al., 1999; Ollmann et al., 2000; Johnson et al., 2010). Expression of p35, the baculovirus-derived inhibitory protein of effector caspases, slightly restored dendritic length of Prel-overexpressing class IV neurons (Hay et al., 1994). However, the degree of recovery was not striking, indicating a minor role of caspase activation in the dendritic loss. Analysis of variance (ANOVA) followed by post-hoc Dunnett's test (versus mCherry-CAAX). (B) Immunoblot analysis revealed promotion of eIF2α dephosphorylation by dPPP1R15 O/E. dPPP1R15 was overexpressed using *hs-Gal4,* which drives Gal4 expression by a heat-inducible Hsp70 promoter. Whole larvae treated with a heat shock (37°C for 1 h) were lysed 10 h after the treatment. Lysates were immunoblotted with anti-phosphorylated eIF2α (P-eIF2α) and anti-eIF2α antibodies. Results of three biological replicates are shown. (C–G) Genetic interactions between O/E or loss-of-function of *prel* and eIF2α phosphorylation-related genes. Quantification of the effects of coexpression of dPPP1R15, S6k[STDETE], and mCherry-CAAX (UAS copy number control) with Prel on the dendritic length of class IV neurons (C). Note that the values of the total dendritic length of neurons that expressed dPPP1R15 and Prel were apparently distributed in a bimodal fashion (see also E). S6k[STDETE]: an active form of S6k (Barcelo and Stewart, 2002). ANOVA followed by post-hoc Dunnett's test (versus mCherry-CAAX). Representative images of the dendritic arbors of Class IV neurons expressing Prel plus mCherry-CAAX (D) or dPPP1R15 (E; see also Fig. S4 A). An example of dendritic arbors (F, left) and quantification of the total dendritic length (F, right) of *prel* mutant class IV MAR CM clones overexpressing dPPP1R15. Representative images (G, left) and quantification of the total dendritic length (G, right) of class IV neurons with Prel O/E plus KD of *Perk, Gcn2,* or *Thor/4EBP.* The amplicon for RNAi of *Perk[HMJ]* line does not overlap with those of other RNAi lines. ANOVA followed by post-hoc Dunnett's test (versus *mCherry[KD]*). (H) Representative images (left) and quantification of the total dendritic length (right) of dPerk-overexpressing class IV neurons. *, $P < 0.05$. Bars, 50 μm.

or at 6 h after the conversion (Fig. 5 I). Collectively, our results imply that Prel O/E–induced mitochondrial dysfunction impairs protein translation in class IV neurons in an eIF2α phosphorylation–dependent manner and that this suppression is stronger in class IV neurons than in other neuronal classes.

Activation of the Ire1 branch of the unfolded protein response in da neurons with or without mitochondrial dysfunction

As demonstrated in Fig. 4 G, *Perk* KD alleviated the dendritic loss of class IV neurons overexpressing Prel. A well-established activator of Perk is ER stress, which activates the unfolded protein response (UPR), consisting of three major branches, referred to as the Ire1, Perk, and ATF6 pathways (Mori, 2009; Walter and Ron, 2011). To better characterize the UPR programs activated by mitochondrial dysfunction in da neurons, we examined the activation of the Ire1 pathway using nuclear localization of X-box binding protein 1 (XBP1)–EGFP as a reporter (Ryoo et al., 2007). Activation profiles of the XBP1 transcription factor, a major downstream target of Ire1, differed between class IV and other classes. Notably, the pathway was transiently activated in the wild-type class IV neurons at early L1 and L2 irrespective of Prel O/E, suggesting physiological activation of the Ire1 pathway. At late L3, it was weakly activated, and only under the genetic condition of Prel O/E (Fig. 6, A, D, and G; and Fig. S4 G). In contrast, the pathway was moderately activated in class I and III

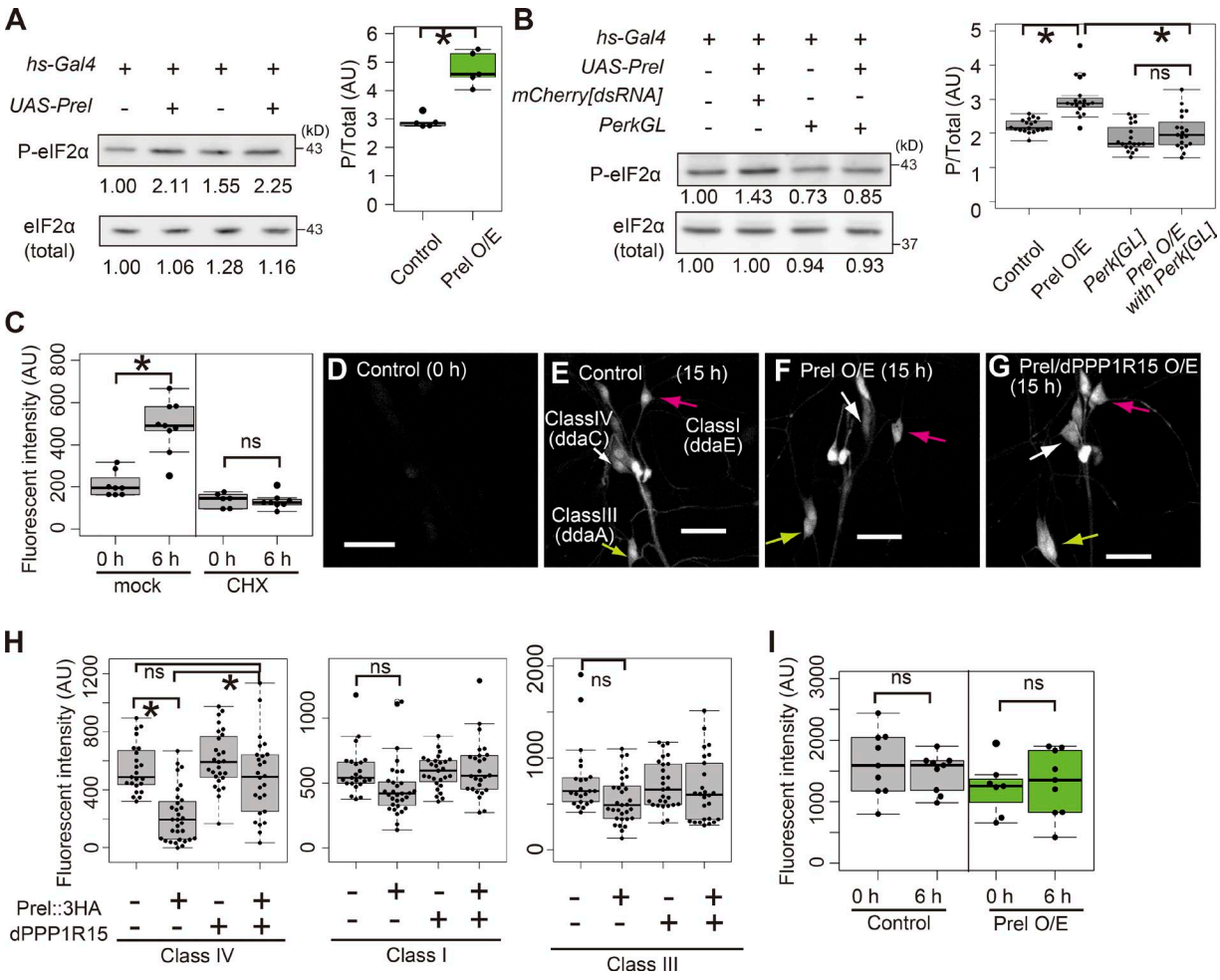

Figure 5. **Differential eIF2α phosphorylation–mediated translational repression in da neurons.** (A) Prel O/E increased P-eIF2α in vivo. Prel was overexpressed by using *hs-Gal4*. Brain lysates of control and Prel-overexpressing adult female flies treated with heat shocks were immunoblotted using antibodies against P-eIF2α or total eIF2α. Immunoblots of two biological replicates are shown and relative values of band intensities are indicated (left). Quantification of the band densities of five biological replicates (right). (B) The increase in the P-eIF2α amount by Prel O/E was partially suppressed by KD of *Perk* (*Perk[GL]*). A representative immunoblot of brain lysates and relative values of band intensities (left). Quantification of the band densities of 19 biological replicates (right). (C) Kaede imaging in da neurons detected translational repression induced by cycloheximide (CHX), an inhibitor of protein translation. Early L3 larvae expressing Kaede in da neurons were prefed with a fly food containing CHX for 4 h before photoconversion (PC). Whole larvae were irradiated with UV light. Intensity of unconverted, green Kaede fluorescence in the soma was quantified. Half of the photoconverted larvae were observed immediately after PC (0 h), and the other half were aged in the fly food containing CHX for 6 h, then observed (6 h). AU, arbitrary units. (D–H) Prel O/E preferentially suppressed representative protein synthesis in class IV neurons. Grayscale images of unconverted Kaede fluorescence in control (D and E), Prel O/E (F), and Prel plus dPPP1R15 coexpression (G). Whole early L3 larvae were irradiated with UV light and aged for 15 h. Arrows indicate the soma of class IV (white), class I (magenta), and class III (yellow) neurons. Bars, 50 µm. Quantification of unconverted Kaede signals in the soma of da neurons (H). Unconverted Kaede signals immediately after and 15 h after PC were quantified. ANOVA with the post-hoc Tukey-Kramer method. (I) Quantification of the intensity of photoconverted Kaede just after conversion (0 h) and 6 h after conversion (6 h) in class IV neurons of either control or Prel O/E. *, $P < 0.05$; ns, not significant.

neurons at early L2 and late L3, but only in the presence of mitochondrial dysfunction (Fig. 6, B, C, and G; and Fig. S4 G). The Prel O/E–associated increase in XBP1-EGFP was more apparent in class III neurons than in class I neurons. The apparent lack of increased XBP1 accumulation in the nucleus in response to Prel O/E in class IV neurons at early L1 and L2 may be caused by negative feedback regulation of Ire1 by XBP1 (Li et al., 2011).

eIF2α phosphorylation is a common mediator of mitochondrial dysfunction–induced dendritic loss resulting from various genetic perturbations

Several genetic conditions in neurons cause mitochondrial dysfunction as well as simplification of dendritic arbors (Chen et al., 2007; Williams et al., 2010; Cheng et al., 2012; Oruganty-Das et al., 2012). When mitochondrial dysfunction is caused by genetic conditions other than aberrant *prel* function, is the malformation of dendrites also mediated by phosphorylation of eIF2α? To address this question, we tested the effects of O/E or loss of function of mitochondrial proteins, including Opa1 (mitochondrially localized dynamin-like GTPase that facilitates the fusion of inner membranes), Opa1[K273A] (a presumably GTPase-negative form of Opa1), Ttm50 (an orthologous protein of yeast Tim50, a component of the mitochondrial protein translocator complex TIM23), TFAM (a mitochondrial high-mobility group protein that binds to mtDNA whose O/E disturbs mitochondrial gene expression and impair ETC function in mouse and fly;

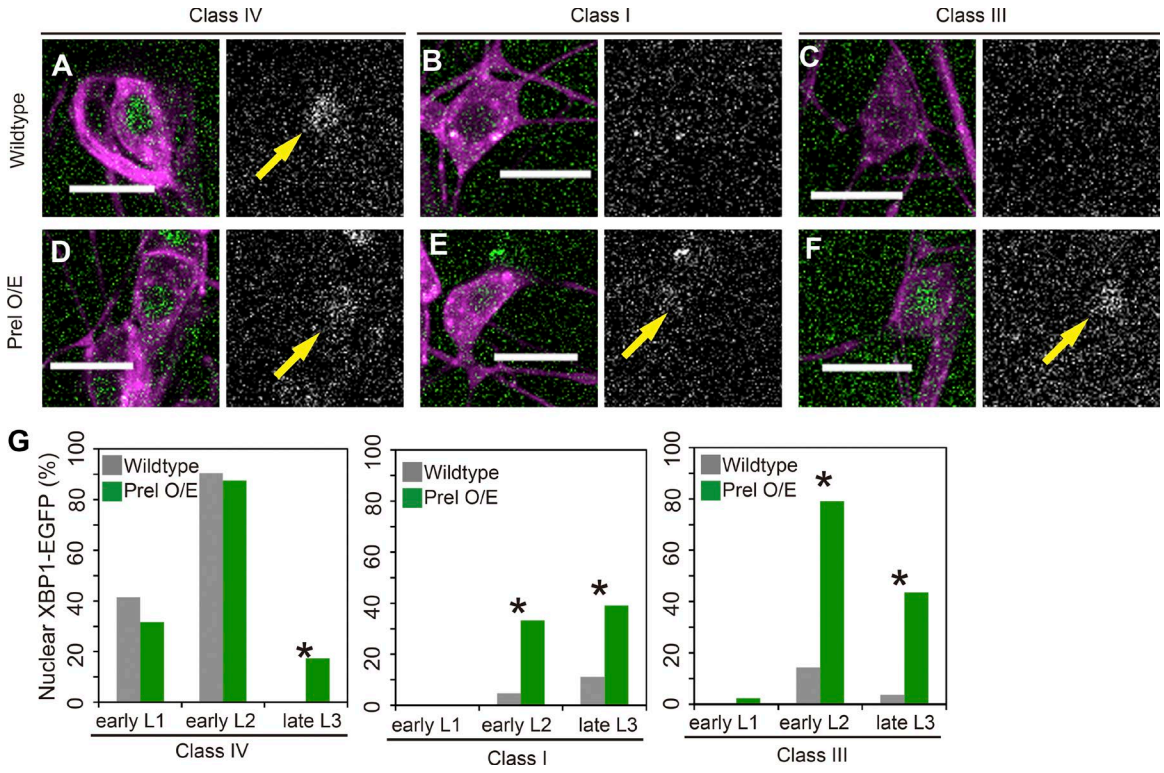

Figure 6. **Prel O/E activates the Ire1 branch of the UPR.** (A–G) The XBP1-EGFP sensor accumulated in the nucleus of da neurons. Representative images of XBP1-EGFP and mCherry-CAAX in the cell bodies of control class IV neurons (A–C) and Prel-overexpressing class IV neurons (D–F) at early L2 (48–52 h AEL). XBP1-EGFP and mCherry-CAAX signals are presented in green and magenta, respectively (A–F, left). Yellow arrows indicate XBP1-EGFP signals accumulated in the nucleus (A–F, right). (G) Quantification of the proportion of neurons with XBP1-EGFP accumulation in the nucleus during larval development. Quantification of fluorescence intensity of XBP1-EGFP in the nucleus at early L2 yielded similar results (see Table S1). *, $P < 0.05$.

Ylikallio et al., 2010; Cagin et al., 2015), and CoVa (a subunit Va of the respiratory complex IV).

Overexpression of Opa1 or Opa1[K273A] in class IV neurons resulted in either large or fragmented spherical mitochondrial morphology, consistent with dominant mitochondrial fusion events and the effect of mutant Opa1 orthologues with reduced GTPase activity on mitochondrial morphology (Fig. 7 A; Olichon et al., 2007). We also tested the *UAS-Ttm50*$^{\#2}$ transgene, because eye-specific O/E is known to cause an apoptosis-dependent rough eye phenotype, suggesting that expression of Ttm50 at a high level could damage mitochondrial function (Sugiyama et al., 2007). Class IV neurons overexpressing Ttm50 displayed predominantly fragmented mitochondria in the cell body (Fig. 7 A). To examine whether each overexpressing condition endowed class IV neurons with an increased dependence on glycolysis for ATP production, we imaged AT[NL] in the presence or absence of an inhibitor of glycolysis (2-DG). Our results showed that all conditions tested increased reliance on glycolysis at late L3 (Fig. S5 A), much like Prel O/E (Fig. 3 A). These results indicated that high expression of Opa1, Opa1[K273A], or Ttm50 impedes ATP supply from mitochondria in class IV neurons.

All of the aforementioned overexpressing conditions significantly reduced the dendritic length of class IV neurons (Fig. 7, B–E); moreover, the reduction of the dendrite length under all of these conditions was partially rescued by coexpressing dPPP1R15 (Fig. 7, F–I). Dendritic losses and their alleviation by dPPP1R15 were also the case with *CoVa[tenured]* mutant and TFAM-overexpressing class IV neurons (Fig. 7, J and K; and Fig. S5 B). Furthermore, *hs-Gal4* dependent O/E of Opa1 or Ttm50 resulted a trend toward an increase in P-eIF2α in adult fly heads (Fig. S5 C). Collectively, these results support the idea that the increase in P-eIF2α is a common mediator of dendritic loss stemming from mitochondrial dysfunction.

These models of mitochondrial stress offered a further opportunity to investigate the relationship between ATP levels in neurons and dendritic loss after mitochondrial malfunction. We imaged ATP levels of class IV neuronal soma at distinct larval stages and found that ATP levels were largely preserved in the individual overexpressing conditions that we tested, whereas Opa1[K273A] O/E slightly decreased the FRET signal only at late L3 (Fig. 7 L).

We also addressed dendritic vulnerability among other da neuronal classes under the same O/E conditions that we used for the class IV neurons. Compared with class IV neurons, dendrite phenotypes of class I and III neurons were milder (Fig. S5, D and E), consistent with our results with aberrant *prel* function (Fig. 1, F–I).

Protein translation consumes a small fraction of ATP expenditure in class IV neurons

What is the physiological significance of increased P-eIF2α in the context of mitochondrial dysfunction? Protein translation is a major energy-consuming process at the organismal level (Rolfe and Brown, 1997). In the *Drosophila* nervous system, transcriptomic analysis of da neurons revealed genes related to protein translation were expressed at higher levels in class IV neurons when compared with whole larvae (Iyer et al.,

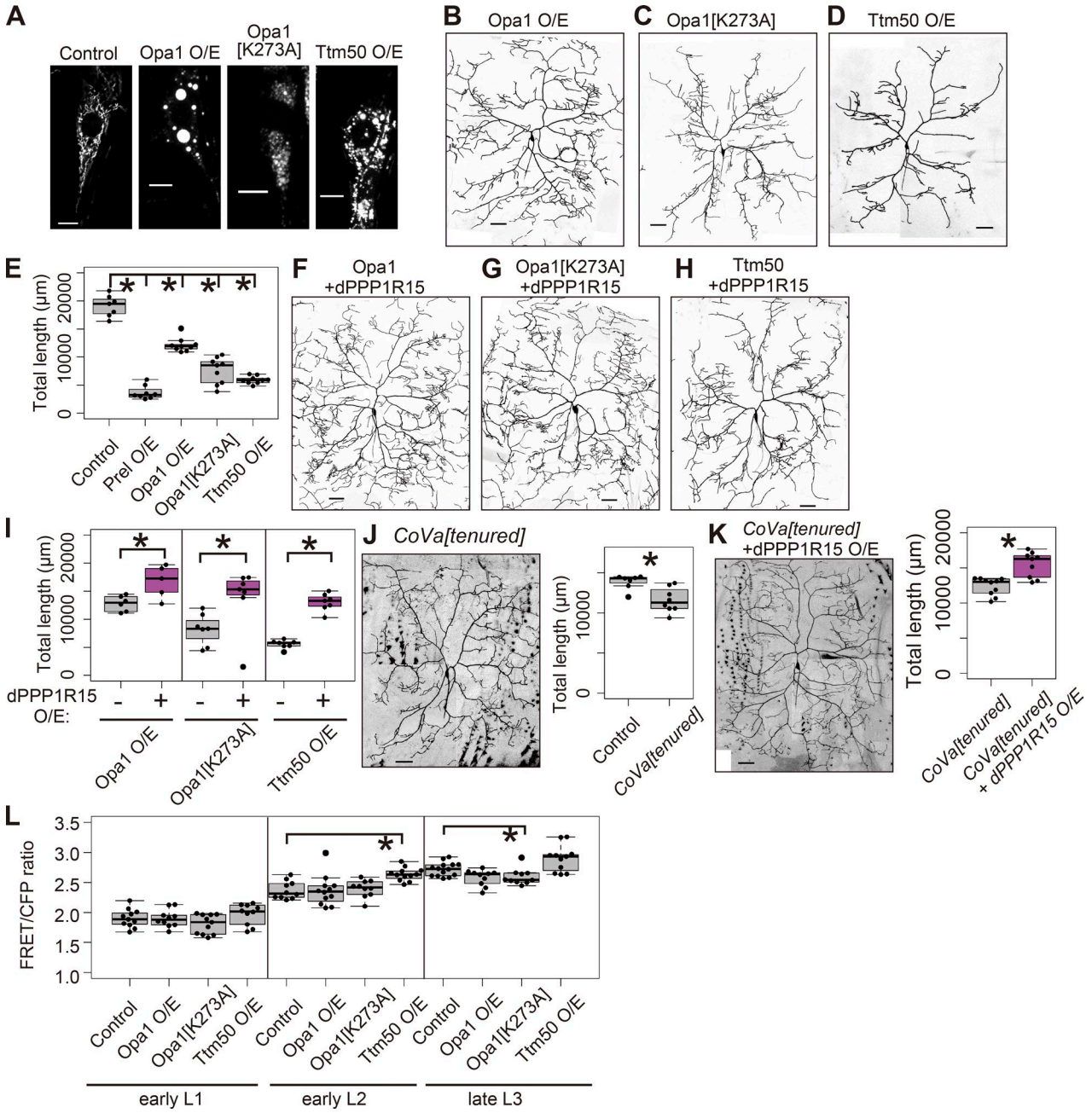

Figure 7. **Increased eIF2α phosphorylation is a common mechanism of dendritic loss induced by various mitochondrial lesions.** (A) Representative images of mitochondrial morphologies in the cell body of class IV neurons expressing Opa1, Opa1[K273A], or Ttm50. Mitochondria were visualized with mitoGFP. (B–I) Expression of Opa1, Opa1[K273A], or Ttm50 in class IV neurons induced dendritic losses, and dPPP1R15 O/E partially prevented dendritic losses. Representative images of dendritic morphologies of class IV neurons expressing Opa1(B), Opa1[K273A] (C), Ttm50 (D), Opa1 plus dPPP1R15 (F), Opa1[K273A] plus dPPP1R15 (G), or Ttm50 plus dPPP1R15 (H). Quantification of the total dendritic length of class IV neurons expressing Opa1, Opa1[K273A], or Ttm50 (E) and expressing dPPP1R15 in conjunction with Opa1, Opa1[K273A], or Ttm50 (I). (J and K) Representative images and quantification of dendritic morphologies of *CoVa[tenured]* mutant class IV neurons (J) and dPPP1R15 overexpressed in *CoVa[tenured]* mutant class IV neurons (K). We generated *CoVa* mutant class IV neurons in the heteromutant background by the MARCM method, which utilizes flippase-based somatic recombination. Loss of function of *CoVa* caused a modest decrease in dendritic length (J). This mild phenotype may be explained by the fact that mutant neurons inherit the enodogenous CoVa protein that was produced before the mitotic recombination event (Liu et al., 2000) and also that mitochondrial OXPHOS complexes display relatively slower turnover rates in the nervous system (Price et al., 2010; Vincow et al., 2013). dPPP1R15 OE in *CoVa[tenured]* mutant class IV neurons restored dendritic patterning (K). (L) Quantification of the FRET signals of AT[NL] in class IV neurons expressing Opa1, Opa1[K273A], or Ttm50 during larval development. *, $P < 0.05$.

2013). Therefore, from a bioenergetic point of view, P-eIF2α–mediated translational repression may provide a way to preserve cellular ATP in class IV neurons.

To examine whether protein translation is a major energy-consuming process in class IV neurons, we evaluated the effect of CHX on the ATP depletion rate after addition of AM plus 2-DG, as we did in Fig. 3 E. We also examined the effect of ouabain, an inhibitor of a major energy consumer in neurons, the Na^+/K^+ ATPase (Howarth et al., 2012). Bath application of CHX did not alter the rate of the reduction in cellular ATP

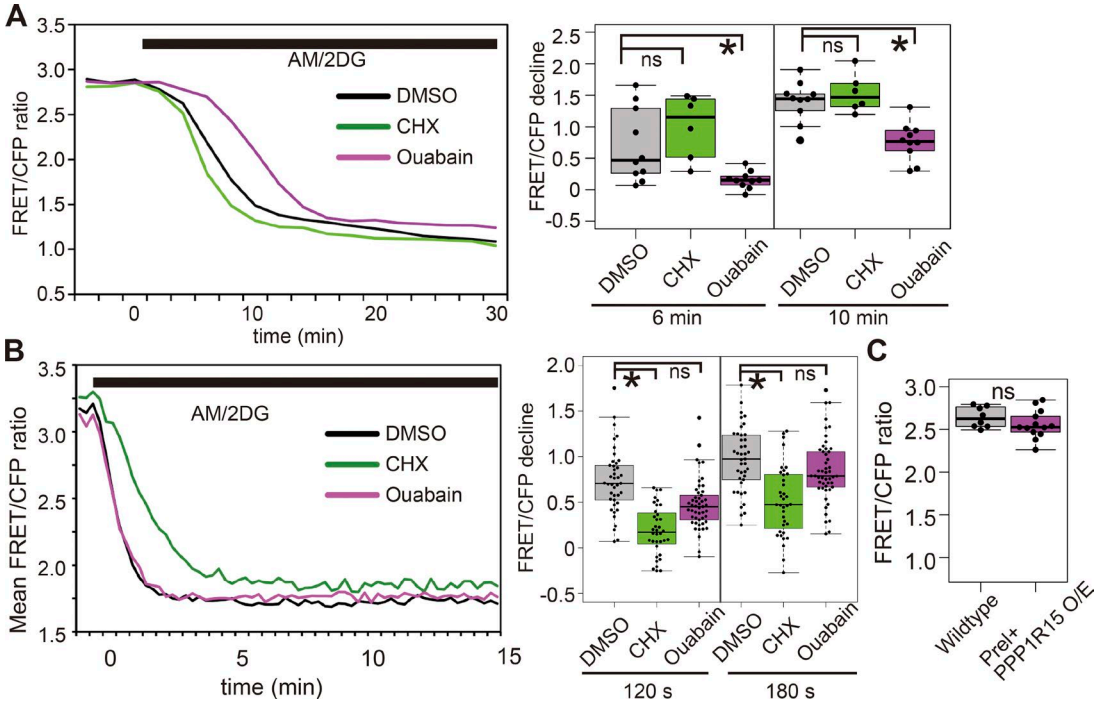

Figure 8. **Protein translation consumes a small fraction of the total ATP budget in class IV neurons.** (A) Real-time imaging of AT[NL] revealed ATP used for protein translation was not high in class IV neurons. Fillet larvae were pretreated with CHX or ouabain for 30 min before the addition of 100 µM AM plus 50 mM 2-DG. The time course of changes in the FRET signals in class IV neurons in the presence of cycloheximide (CHX) or ouabain, an inhibitor of Na^+/K^+ ATPases (left). Quantification of the decline of FRET signals in the soma of class IV neurons expressing AT[NL] treated with DMSO (control), 25 mM CHX, or 50 mM ouabain (right). See also Fig. S3 E. (B) Real-time imaging of AT[NL] revealed ATP used for protein translation was high in *Drosophila* BG2-c2 cells. The cells transiently expressing AT[NL] were treated with 20 µM AM and 20 mM 2-DG in conjunction with 20 µM CHX or 50 mM ouabain. DMSO, CHX, or ouabain was added 30 min before the addition of AM plus 2-DG. Time courses of changes in the FRET signals in BG2-c2 cells in the presence of CHX or ouabain are shown (left). Quantification of decline of FRET signals in BG2-c2 cells expressing AT[NL] treated with DMSO (control), 20 µM CHX, or 50 mM ouabain (right). See also Fig. S3 F. (C) Quantification of the FRET signals of AT[NL] in the soma of wild-type class IV neurons and class IV neurons with prel plus dPPP1R15 coexpression. *, $P < 0.05$; ns, not significant.

levels in class IV neurons; in contrast, ouabain significantly slowed the rate of decline (Figs. 8 A and S3 E). We compared class IV neurons to DmBG2-c2 cells. Because this cell line is highly proliferative, we expected that protein translation would consume a large fraction of ATP expenditure to meet the intense demand for protein synthesis. When we treated BG2-c2 cells with AM plus 2-DG, cellular ATP levels dropped instantaneously (Figs. 8 B and S3 F). As we expected, treatment with CHX substantially slowed the rate of ATP consumption, whereas ouabain failed to affect the rate of ATP consumption. These data indicate that ATP used for protein translation is a large fraction of the total ATP consumption in Dm BG2-c2 cells but a small fraction of the ATP expenditure in class IV neurons. Furthermore, Prel and dPPP1R15 coexpression in class IV neurons did not affect cellular ATP levels (Fig. 8 C). Thus, P-eIF2α–dependent translational repression does not appear to be important for the ATP preservation in class IV neurons after mitochondrial dysfunction.

Discussion

Dendrite loss induced by mitochondrial dysfunction can occur while neuronal ATP levels are preserved in physiologically relevant ranges

Decreased ATP levels in neurons can act as a cellular signal from dysfunctional mitochondria, and the essential roles of ATP depletion have been proposed not only in neuronal survival but also in presynaptic deficits and axonal degeneration processes (Verstreken et al., 2005; Koike et al., 2008; Morais et al., 2009; Yang et al., 2015). Furthermore, in presynaptic terminals of primary cultured rodent neurons, relatively high ATP levels are required for sustained endocytosis (Rangaraju et al., 2014; Pathak et al., 2015). In this study, we used FRET-based ATP sensors to investigate whether decreased ATP content was correlated with dendritic patterning defects induced by various genetic manipulations to perturb mitochondrial functions. We found ATP levels are largely preserved in class IV neurons at stages when dendritic patterning defects and dendritic destabilization are detected. Thus, our results add weight to the idea that ATP depletion is not a direct cause of dendritic loss in class IV neurons.

A few studies have applied ATP sensors to neurons with mitochondrial dysfunction (Fukumitsu et al., 2015; Pathak et al., 2015; Shields et al., 2015). In primary cultured hippocampal neurons, loss of function of NDUFS4 (a subunit of the respiratory complex I) or Drp1 (a major mitochondrial fission regulator) did not affect the basal FRET signal of ATeam[YEMK] (an ATeam variant) at synaptic boutons; glycolysis compensated for the mitochondrial dysfunction (Pathak et al., 2015: Shields et al., 2015). These results are consistent with our results obtained from the dendrites and cell bodies of da neurons. Our ATP imaging also revealed reduced ATP consumption in class IV neurons with Prel O/E. Although the exact means by which the class IV neurons reduced ATP consumption was not estab-

lished in this study, we speculate that the dendritic loss may contribute to the reduction of the energy budget by reducing membrane surface area of the shortened arbors. This idea is supported by the fact that cell membrane–related processes, including ion movements across the membrane and phospholipid metabolism, are energy intensive (Engl and Attwell, 2015) and that the Na^+/K^+ ATPase is a major ATP consumer in class IV neurons, as we demonstrated.

We note a few caveats in our ATP imaging in da neurons. First, our ATP imaging is qualitative rather than quantitative because of the lack of in-cell calibration experiments for AT[NL]. We could not perform such a calibration because cell permeabilization procedures, to our knowledge, have not been established in *Drosophila*. Such calibration in fly cells could allow us to interpret the signal in a quantitative or semi-quantitative manner (Rangaraju et al., 2014; Pathak et al., 2015). Second, the signal of AT[NL] was apparently affected in an ATP-independent manner. Recently, Yaginuma et al. reported the signals of FRET probes, consisting of two separate fluorescent proteins that differ in maturation half time and can be independently degraded, can be affected by the status of fluorescent proteins regardless of binding to target molecules (Yaginuma et al., 2014). The ATP-independent increases in the signals we detected can be explained by the elapsed time from the onset of expression and by the increase of P-eIF2α, both of which decrease a fraction of newly translated, half-mature ATeams with the immature acceptor in neurons. Using recently developed circularly permutated fluorescent protein–based ATP probes may obviate these difficulties (Yaginuma et al., 2014). Third, we could not address ATP levels at the tips of dendritic arbors because of decreased fluorescence of the probe and strong autofluorescence of the epidermis. Therefore, we cannot exclude the possibility that mitochondrial dysfunction leads to ATP depletion at the tips. As reduced ATP levels in distal dendrites have been reported in cultured Purkinje cells (Fukumitsu et al., 2015), it would be interesting to monitor ATP levels with modified ATP biosensors that are able to efficiently localize to more distal regions of dendritic arbors in da neurons.

eIF2α phosphorylation contributes to the dendritic loss induced by mitochondrial dysfunction

Dendritic pathology associated with mitochondrial dysfunction has been reported in many neuronal types, and altered dynamics in cytoplasmic Ca^{2+} and the actin cytoskeleton are currently proposed as causal molecular mechanisms (Dickey and Strack, 2011; Cichon et al., 2012; Fukumitsu et al., 2015; Maltecca et al., 2015). In this study, we found that P-eIF2α–mediated translational repression contributes to dendritic loss after mitochondrial malfunction, which is, to our knowledge, a new addition to the previously proposed mechanisms. As dPPP1R15 O/E did not rescue severe fragmentation of mitochondria in class IV neurons overexpressing Prel, dendritic loss might be alleviated without the recovery of mitochondrial function, hinting at a critical role of the downstream eIF2α-mediated stress signaling in dendritic loss.

A close association between mitochondrial dysfunction and eIF2α phosphorylation–mediated translational attenuation has been demonstrated by genetic or pharmacological OXP HOS inhibition, which led to increased P-eIF2α through various eIF2α kinases (Janssen et al., 2009; Baker et al., 2012; Evstafieva et al., 2014; Michel et al., 2015). Furthermore, elevations of P-eIF2α have frequently been reported in various tissues from patients and cellular and animal models of PD (Ryu et al., 2005; Hoozemans et al., 2007; Mutez et al., 2014). It has been shown that the elevated P-eIF2α in *Drosophila pink1* or *parkin* mutants is partially suppressed by KD of *Perk* (Celardo et al., 2016). We demonstrated that KD of *Perk*, but not *Gcn2*, alleviated the dendritic loss, and Prel O/E also induced activation of the Ire1 branch of the UPR pathways in da neurons. Our data suggest that mitochondrial dysfunction induces activation of the UPR in da neurons, and one of the UPR branches (i.e., Perk, which phosphorylates eIF2α) elicits the dendritic pathology. Mitochondria physically and functionally interact with the ER, and functions of each organelle are interdependent (Naon and Scorrano, 2014; Senft and Ronai, 2015). However, how altered mitochondrial functions and structure cause the UPR is still unclear (Naon and Scorrano, 2014).

Recently, associations of the UPR and dendrite patterning have been reported. Loss of function of Ire1 in *Caenorhabditis elegans* PVD neurons gives rise to less branched distal dendritic trees through inefficient targeting of a trans-membrane protein DMA-1, which is necessary for distal dendritic branching and patterning (Wei et al., 2015). To meet increasing protein load into the ER, Ire1 is transiently activated during normal development when dendrites elongate and branch out, which is compatible with transient activation of the Ire1 pathway in class IV neurons. In *Drosophila* olfactory neurons, genetically induced ER stress reduces ephrin on the neuronal cell surface, leading to a dendritic mistargeting phenotype (Sekine et al., 2013). In contrast to these two models, dendritic loss in our model was not likely caused by impaired protein-folding capacity in the ER and resultant deregulated localization of key transmembrane proteins. This is primarily because the dendritic phenotype in this study was recovered in general, but did not become worse, by the restoration of general translation, which may increase protein load in cells and create a less favorable environment for protein folding in the ER. Rather, we speculate that attenuated protein synthesis is a cause of the dendritic losses we observed. In support of this notion, dPerk O/E is sufficient for dendritic undergrowth, and the requirement of general protein synthesis in dendrite patterning has been demonstrated in several studies (Chihara et al., 2007; Koike-Kumagai et al., 2009; Niehues et al., 2015).

The physiological significance of eIF2α phosphorylation in mitochondria-related diseases is not firmly established. Increased P-eIF2α may exert detrimental effects on neuronal function, as demonstrated in animal models of various neurodegenerative diseases (Kim et al., 2014; Scheper and Hoozemans, 2015) and a neuropathological effect on dendritic patterning as we observed. Conversely, the severe dendritic loss that was sometimes observed in Prel plus dPPP1R15 or TFAM plus dPPP1R15 coexpressing class IV neurons suggests a neuroprotective role of elevated P-eIF2α in response to mitochondrial dysfunction. Our ATP imaging indicates that ATP conservation through translational attenuation is unlikely to be the primary mode to protect class IV neurons, being consistent with a small contribution of protein synthesis to the total energy budget of mammalian nervous systems (Engl and Attwell, 2015; Engl et al., 2016). One possible mediator of the neuroprotective role of eIF2α phosphorylation is ATF4, whose translation is promoted by increased P-eIF2α, and ATF4 has been reported to be protective in response to neuronal mitochondrial

dysfunction (Bouman et al., 2011; Sun et al., 2013). Further investigations are required to elucidate the mechanistic basis of the dichotomy between neurotoxic and neuroprotective roles of P-eIF2α. At the organismal level, translational attenuation via eIF2α phosphorylation may act as a prosurvival signal. In the body, there are other cell types that have high ATP demands for protein synthesis, as proliferative culture cell line BG2-c2 does. When ATP consumption is restricted in such cell types as BG2-c2, the reduced energy budget of the whole organism may lead to sparing of internal energy substrates and thereby enable organs with high energetic costs whose function is necessary for survival of individuals, including the nervous system, to preferentially use energy, at least in transient energy crises (Niven and Laughlin, 2008).

Differences in protein synthesis activities of neuronal subtypes underlie the selective vulnerability of the dendritic arbors of da neurons to mitochondrial dysfunction

One of the major unanswered problems in the research of mitochondria-related diseases is the vulnerability of selective neuronal types. Our representative protein synthesis imaging demonstrated that class IV neurons incurring mitochondrial stress suffered from more severe translational suppression than other classes, which argues that differential suppression at the level of protein translation could be a critical contributor to vulnerability of some neuronal types to mitochondrial dysfunction. Interestingly, several genes encoding translational regulators are causative for PD, and recent studies have implicated protein translation as a key part of the pathogenesis of PD (Lu et al., 2014; Taymans et al., 2015).

How does the differential translational attenuation occur in da neurons after mitochondrial dysfunction? One possible scenario is that the physiological UPR in class IV neurons underlies the differential translational repression by way of differences in basal P-eIF2α levels and/or the efficiency of eIF2α phosphorylation. Further investigations to characterize UPR in developing class IV neurons are required. Physiological activation of the UPR during development is finely tuned in various cell types, including neurons (Rutkowski and Hegde, 2010). The differential importance of the physiological UPR among neuronal subtypes and during neural development is likely to be evolutionary conserved (Zhang et al., 2007; Naidoo et al., 2008; Valdés et al., 2014).

Although our data suggest a key role of differential translational attenuation in selective vulnerability to mitochondrial dysfunction, other factors must contribute to the fragility through protein translational activity—or independently. Although protein synthesis is universally essential for cellular survival and function, activity of and reliance on protein translation differ in developmental stages, cell types, or even subcellular locations (Sutton and Schuman, 2006; Scheper et al., 2007; Remmen et al., 2011). It will be interesting to investigate whether cells and cellular activities with higher demands for protein synthesis are preferentially impaired by mitochondrial dysfunction. Higher demands for ATP or severe OXPHOS impairment in some neuronal types can be an underlying factor for strong mitochondrial stress signaling (Burman et al., 2012; Pacelli et al., 2015). Future studies to evaluate ATP consumption in various neuronal types at single-cell resolution in vivo will improve our understanding of differential energy demands in neuronal subpopulations.

Materials and methods

Fly strains

Flies were raised on standard cornmeal-based *Drosophila* medium at 25°C. To acquire precisely staged larvae, embryos were collected on apple agar plates with a drop of yeast paste, and flies were aged at 25°C. Mutant clone neurons were generated using mosaic analysis with a repressible cell marker (MARCM; Wu and Luo, 2006), *Gal4*$^{109(80)}$ (Gao et al., 1999), *Gal4[5–40]* (Song et al., 2007), and *SOP-FLP* fly lines (Shimono et al., 2014). For Prel O/E experiments, *UAS-prel::3HA* (Tsubouchi et al., 2009) and the following class-specific Gal4 drivers were used: *Gal4[2–21]* for class I (Grueber et al., 2003), *Cal4[c161]* for class III (Shepherd and Smith, 1996), and *ppk-Gal4* for class IV (a gift from the Yuh-Nung Jan laboratory, University of California, San Francisco, San Francisco, CA). To express Kaede, we used *Gal4[21–7]* (Song et al., 2007) as a driver because it induced UAS transgenes with relatively similar expression levels between classes of da neurons during larval development (Fig. S4 F). *UAS-dPPP1R15* and *UAS-dPerk* (Malzer et al., 2010) lines were gifts from S. Marciniak (University of Cambridge, Cambridge, England, UK). *UAS-Ttm50*$^{\#2}$ was a gift from Y. Nishida (Nagoya University, Nagoya, Japan). *CoVa[tenured]* is a null allele for the *CoVa* gene (Mandal et al., 2005). Other strains used in this study were provided by stock centers. Genotypes used in each experiment are summarized in Table S2.

DNA plasmids and transgenic flies

To generate the *UAS-dOpa1::3HA* fly line, the full-length DNA sequence of *dOpa1* amplified from cDNA obtained from our *y* w** stock was cloned into the pUAST plasmid (Brand and Perrimon, 1993). pUAST-dOpa1[K273A]::3HA was generated by site-directed inverse-PCR mutagenesis with the following primers (where the underlined text indicates mutated sequences): 5′-GCGCGACCTCTGTCCTGGAATCC-3′ (forward) and 5′-CGCTGCTCTGATCTCCCACTACC-3′ (reverse).

The *Opa1[K273A]* transgene harbors a single amino acid substitution in a lysine residue that is evolutionary conserved in dynamin-family GTPases and essential for the GTPase activity of human Opa1 (Griparic et al., 2004).

To generate transgenic flies, constructs were injected with a transpose plasmid pTurbo (a gift from K. Tatei, Gunma University, Maebashi, Japan) into our *y* w** stock using a standard germline transformation technique.

Chemicals

2-DG (D-8375; Sigma-Aldrich), AM (ALX-380-075; Enzo Life Sciences), oligomycin (ALX-380-037; Enzo Life Sciences), and CCCP (S2759; Sigma-Aldrich) were used to inhibit ATP production pathways. 2-NBDG (2-deoxy-2-[(7-nitro-2,1,3-benzoxadiazol-4-yl) amino]-D-glucose; 11046, Cayman Chemical) was used to evaluate glucose uptake of class IV neurons. CHX (06741-91; Wako Pure Chemical Industries) and Ouabain (Alx-350-666; Enzo Life Sciences) were used to inhibit protein translation and Na/K ATPase, respectively. Diethyl ether (055-01155; Wako Pure Chemical Industries) was used for larval anesthesia.

Dendrite imaging and quantification of total dendritic length

For whole-mount live dendrite imaging, larvae were mounted in glycerol (50% or 80% vol/vol) under coverslips and kept at 4°C to attenuate larval movements. Larvae were imaged using a confocal microscope (C-1; Nikon) with a 40×/1.30 NA objective. 2D projections of Z stacks were used for quantification. Images were skeletonized and quantified with ImageJ (Schneider et al., 2012; Iyer et al., 2013). The pixel intensity for neuronal images was thresholded and converted to binary

images in Image J. Remained background noise and structures with autofluorescence were eliminated by filtering with the Analyze Particle plugin in ImageJ (size, 10 μm^2 to infinity; circularity, 0–0.35). Then, images were skeletonized using the Skeletonize3D plugin and analyzed using the Analyze Skeleton plugin in ImageJ. Skeletons of the cell body and axon were deleted with the brush tool in ImageJ. When necessary, traces of dendritic arbors were made by hand using Illustrator (Adobe).

For time-lapse imaging of dendritic terminals, early L2 larvae (46–50 h AEL) were collected and anesthetized with diethyl ether (Sugimura et al., 2003). Larvae were raised on apple agar plates with a yeast drop. Early L2 larvae were rinsed in PBS and anesthetized in a glass Petri dish filled with diethyl ether. The larvae were mounted in 50% glycerol under coverslips and immediately observed. After dendrite imaging, the larvae were recovered from anesthetization in PBS supplemented dry yeast (Oriental Yeast Co.). After recovery from anesthesia, larvae were aged for 24 h on apple agar plates with a drop of yeast paste.

FRET imaging and analysis

FRET-based ATP biosensors, ATeams, consist of mseCFP as a FRET donor, cp173-mVenus as a FRET acceptor, and the epsilon subunit of *Bacillus subtilis* FoF1 ATP-synthase, which links the donor with the acceptor. Binding of ATP to the epsilon subunit induces its large conformational change into a folded form, resulting in an increase in FRET efficiency (Imamura et al., 2009). In FRET imaging, fly larvae and *Drosophila* cell lines were kept at 25°C, where the probe is optimized to detect changes in physiologically relevant ATP levels (Tsuyama et al., 2013)

Flies and cells expressing ATeams were imaged using a C-1 confocal microscope controlled by EZ C-1 software (Nikon) with a 440-nm solid-state laser (Melles Griot) for excitation and a 457-dclp dichroic mirror and two emission filters (485/40 for CFP and 530LP for YFP-FRET; Chroma Technology Corp.) A series of z-sections was projected if necessary. To subtract background signals, we selected a background region adjacent to regions of interest (ROIs). The mean fluorescent intensity of the background regions was subtracted from that of the ROI. FRET signals (FRET/CFP emission ratio) within ROIs were calculated by dividing mean intensity of FRET emission by that of the CFP emission using Microsoft Excel (Microsoft). Ratio images were generated in intensity modulated display (IMD) using MetaMorph (Molecular Devices).

Cultured cells expressing ATeams were adhered to glass bottom dishes covered with concanavalin A (037-08771; Wako Pure Chemical Industries) for S2 cells or poly L-lysine (P4707; Sigma-Aldrich) for DmBG2-c2 cells, incubated for 8 to 12 h at 25°C and imaged using a C-1 confocal microscope with a 20×/0.8 NA objective. S2 cells and Dm BG2-c2 cells were maintained in Schneider's *Drosophila* medium (21720; Gibco and Thermo Fisher Scientific) supplemented with 10% FBS and penicillin/streptomycin and M3 medium (S3652; Sigma-Aldrich) supplemented with 10% FBS, penicillin/streptomycin, and 10 μg/ml insulin (I6634; Sigma-Aldrich), respectively. Cells for imaging were transiently cotransfected with pDA (actin-Gal4; a gift from S. Yoshiura, RIKEN Center for Developmental Biology, Kobe, Japan) and specific pUAST-based plasmids. HilyMAX (Dojindo) and Effectene (QIAGEN) were used for DNA transfection of S2 cells and BG2c-2 cells, respectively.

For whole-mount FRET imaging, larvae were mounted as for dendrite imaging and immediately imaged. For imaging of fillet larval preparations, late L3 larvae were dissected in HL6 medium supplemented with 5 mM D-glucose using a magnet chamber–based method (Ramachandran and Budnik, 2010). Original HL6 medium contains 80 mM trehalose as a sole sugar for an energy substrate (Macleod et al., 2002). We added D-glucose to the medium, because fly larval hemolymph contains D-glucose and high-trehalose is insufficient to maintain basal oxygen consumption of Locust CNS in vitro (Strang and Clement, 1980; Echalier, 1997). In the saline containing glucose and trehalose, class IV neurons of filleted larvae undergo spontaneous firing activities at relatively low frequency (Xiang et al., 2010; Im et al., 2015). We selected the whole soma including the nucleus as the ROI.

We did not perform direct comparisons of FRET signals between different developmental stages for the following reason. In wild-type class IV neurons, the signal of AT[NL] apparently increased as larval development proceeded (Fig. 2 D, control). Note that we used different parameter sets (i.e., higher laser power and detector gain) for confocal imaging of biosensors in da neurons at early L1 because of lower expression levels of probes at this stage than in later larval stages. These settings might slightly affect the signals at early L1. Importantly, in AT[RK] imaging, a similar trend toward increased FRET signals during development was detected (Fig. 2 E). Thus, the increasing FRET signals of AT[NL] during the course of larval development may be at least partly caused by ATP-independent effects. We speculate that the increased signals may stem from decreases in the proportion of immature FRET probes (i.e., ATeams with mature mseCFP and immature cp173-mVenus; Yaginuma et al., 2014), thus eliminating a pool of probes with an intrinsically low FRET/CFP emission ratio. We also detected ATP-independent changes of ATeams in class IV neurons in the presence of AM (Fig. 2 B, arrowheads). These additional drops were often observed in class IV neurons in the presence of AM. The neurons with the additional drops underwent severe morphological alterations (e.g., dendritic varicosity formation and abnormal accumulation of probes in the nucleus), suggesting a failure to maintain cellular homeostasis, which may result in the ATP-independent change in the signals.

2-NBDG uptake assay

Late L3 larvae were dissected in HL6-based medium supplemented with 5 mM glucose. Then, they were incubated in a low-sugar HL6-based medium that contained 8 mM trehalose and no glucose for 10 min to facilitate glucose uptake, followed by replacement with the 8 mM trehalose HL6 medium containing 500 nM 2-NBDG for 5 min. Larvae were then washed five times in HL6 medium containing 5 mM glucose and immediately imaged using a C-1 confocal microscope with a 60×/1.40 NA objective.

Kaede imaging

To express Kaede, we used *Gal4[21–7]* as a driver (Song et al., 2007). Early L3 larvae (~75–80 h AEL) expressing Kaede were collected and photoconverted by using a macro zoom microscope (MVX10; Olympus) with a mercury lamp and a band-pass filter letting through ultraviolet wavelength (U-MWU2; Olympus). While being photoconverted, larvae were floating on Schneider's *Drosophila* medium containing 15% sucrose (wt/wt) in a chamber. Approximately half of the photoconverted larvae were immediately observed to measure the remaining unconverted Kaede fluorescence. The rest of the larvae were aged in an instant *Drosophila* food (Formula 4-24; Carolina). We used a C-1 confocal microscope with a 20×/0.75 NA objective for imaging. We quantified Kaede fluorescence in the cell body of da neurons using EZ C-1 software (Nikon). For cycloheximide treatments, larvae were fed with an instant food made with water containing 25 mM cycloheximide. Larvae were prefed for 4 h before PC and, after PC, aged in the instant food containing cycloheximide for 6 h. For the Prel plus PPP1R15 coexpression experiment, the mean value of fluorescent signals immediately after PC was subtracted from the signals of individual neurons at 15 h after PC in each condition.

Mitochondria and XBP1-EGFP imaging

Late L3 larvae were mounted as for dendrite imaging and immediately imaged using a C-1 confocal microscope with a 60×/1.40 NA objective.

To assess gene expression levels in da neurons, we used several nonpreferring lines that harbor *Gal4* insertions in upstream regions of the translation start sites of various genes, which are expected to mimic endogenous gene expression patterns and levels. Those nonpreferring lines were crossed to our *UAS-mitoGFP UAS-myr-mRFP* stock. Mitochondrial gene expression was defined as GFP intensity per cytoplasmic area in the cell body. GFP fluorescence intensities were normalized to relative expression levels between each class of da neurons in the same hemisegment. Our results showed that mitochondrial gene expression levels in class IV neurons were higher than those in class I and III neurons (Table S1, A–F in p10); and we also measured glycolytic gene expression levels in da neurons (Table S1, G-I in p10) and *Ubi-Gal4*-dependent expression levels in da neurons (Table S1, J in p10). We also confirmed other Gal4 enhancer trap lines of *blw* (NP2316 and NP2527), *PyK* (NP2224), *NC73EF* (NP6535), and *HexA* (NP0735) exhibited similar relative expression levels to NP2718, NP2635, NP0607, and NP6120, respectively, in each class.

The XBP1-GFP marker was coexpressed with mCherry-CAAX in da neurons using *Gal4[21–7]*. The region of the nucleus was determined by the fluorescence of mCherry-CAAX.

Immunoblot analysis

To activate *hs-Gal4*–dependent *UAS-dPPP1R15* expression, late L2 larvae were heat-shocked at 37°C for 1 h and lysed 10 h later. To overexpress Prel, young adult female flies (0–5 d after eclosion) were treated at 37°C for 45 min every 12 h. Flies were sacrificed 8 h after the fifth heat shock treatment. Fly brains were collected with metal sieves (Tian et al., 2013). Flies were frozen and stored in centrifuge tubes at –80°C. Fly heads were collected using two metal sieves with a mesh opening of 355 and 710 µm (Nonaka Rikaki). The prechilled sieves were stacked with the larger mesh sieve, which let through fly heads but not thoraces and abdomens, on the top. Frozen fly heads were separated from their thoraces by shaking tubes and were dropped on the top sieve, and the sieves were banged on a desk. Fly heads retained on the bottom sieve were collected. Fly brains and larvae were lysed in standard Laemmli sample buffer. Approximately 5 or 7.5 µg (for total eIF2α detection) or 15 µg (for P-eIF2α detection) protein was loaded per lane for PAGE. Antibodies against eIF2α (Ab26197, rabbit polyclonal; Abcam) and P-eIF2α (D9G8, rabbit monoclonal; Cell Signaling Technology) were used for immunoblotting (1:2,500 and 1:5,000 dilutions of the antibodies as supplied, respectively). An immunoreaction enhancer (Signal Enhancer Hikari; Nacalai) was used. A peroxidase-conjugated secondary antibody (NA943V; GE Healthcare) was used for detection, and signals were visualized using an LAS-3000 imaging system (Fujifilm). The density of bands was quantified with ImageJ.

Statistical analysis

Microsoft Excel and R (R Core Team) were used for data analysis. We adopted an α level of 0.05. Mean value, 95% confidence interval, p-value, and sample size are summarized in Table S1.

Online supplemental material

Fig. S1 shows mild dendritic losses of class I and III neurons with altered *prel* function and uptake of 2-NBDG by glial cells that wrap around class IV neurons of the control genotype. Fig. S2 shows ATeam1.03NL (AT[NL]), FRET imaging of neurons of the wild-type genotype in the presence of inhibitors of ATP production pathways, and imaging of control or Prel O/E neurons at early L1. Fig. S3 shows responses of individual class IV neurons of O/E or loss of function of *prel* to inhibitors of ATP production pathways. Fig. S4 shows genetic interaction between Prel and dPPP1R15, levels of eIF2α phosphorylation in cultured cells in the presence of various mitochondrial inhibitors, and activation of the XBP1 pathway in wild-type neurons. Fig. S5 shows the FRET imaging, levels of eIF2α phosphorylation, and dendrite length of Opa1-, Opa1[K273A]-, or Ttm50-overexpressing da neurons and the genetic interaction between TFAM and dPPP1R15. Table S1 shows statistical tests used, exact p-values, 95% confidence intervals, and sample sizes in figures and gene expression analysis in da neurons with Gal4 enhancer lines. Table S2 shows genotypes used in each experiment.

Acknowledgments

Reagents, genomic datasets, and/or facilities were provided by the Kyoto Stock Center (Drosophila Genomics Resource Center), the Bloomington Stock Center, Vienna *Drosophila* Resource Center, the TRiP at Harvard Medical School (National Institutes of Health, National Institute of General Medical Sciences grant R01-GM084947), the *Drosophila* Genomics Resource Center, FlyBase, S. Marciniak, Y. Nishida, T. Igaki, M. Miura, K. Ui-Tei, and S. Yonehara. We also thank R.E. Itoh for advice on FRET imaging, J. Hejna for polishing the manuscript, and K. Oki, J. Mizukoshi, and M. Futamata for technical assistance.

This work was supported by a grant from the programs Grants-in-Aid for Scientific Research on Innovative Areas "Mesoscopic Neurocircuitry" (22115006 to T. Uemura), a grant from Takeda Science Foundation to T. Uemura, a Grant-in-Aid for Scientific Research (C) to T. Usui (24500410), a grant from the programs Grants-in-Aid for Scientific Research on Innovative Areas "Brain Environment" to T. Usui (24111525), a Grant-in-Aid for Scientific Research (B) to H. Imamura (26291027), and the Platform Project for Supporting in Drug Discovery and Life Science Research (Platform for Dynamic Approaches to Living System) from the Ministry of Education, Culture, Sports, Science and Technology and the Japan Agency for Medical Research and Development. T. Tsuyama and A. Tsubouchi were recipients of Japan Society for the Promotion of Science Research Fellowship for Young Scientists.

The authors declare no competing financial interests.

Author contributions: T. Tsuyama, A. Tsubouchi, and T. Uemura conceived the project. T. Tsuyama performed experiments and analyzed data. A. Tsubouchi, T. Usui, and H. Imamura provided critical guidance for plasmid construction, generation of transgenic flies, dendrite imaging, cell cultures, and ATeam probes. T. Tsuyama and T. Uemura wrote the paper, incorporating suggestions from all authors.

Submitted: 15 April 2016
Revised: 30 November 2016
Accepted: 19 January 2017

References

Adachi-Yamada, T., M. Nakamura, K. Irie, Y. Tomoyasu, Y. Sano, E. Mori, S. Goto, N. Ueno, Y. Nishida, and K. Matsumoto. 1999. p38 mitogen-activated protein kinase can be involved in transforming growth factor beta superfamily signal transduction in *Drosophila* wing morphogenesis. *Mol. Cell. Biol.* 19:2322–2329. http://dx.doi.org/10.1128/MCB.19.3.2322

Baker, B.M., A.M. Nargund, T. Sun, and C.M. Haynes. 2012. Protective coupling of mitochondrial function and protein synthesis via the eIF2α kinase GCN-2. *PLoS Genet.* 8:e1002760. http://dx.doi.org/10.1371/journal.pgen.1002760

Barcelo, H., and M.J. Stewart. 2002. Altering *Drosophila* S6 kinase activity is consistent with a role for S6 kinase in growth. *Genesis.* 34:83–85. http://dx.doi.org/10.1002/gene.10132

Bollen, M., W. Peti, M.J. Ragusa, and M. Beullens. 2010. The extended PP1 toolkit: Designed to create specificity. *Trends Biochem. Sci.* 35:450–458. http://dx.doi.org/10.1016/j.tibs.2010.03.002

Bouman, L., A. Schlierf, A.K. Lutz, J. Shan, A. Deinlein, J. Kast, Z. Galehdar, V. Palmisano, N. Patenge, D. Berg, et al. 2011. Parkin is transcriptionally regulated by ATF4: Evidence for an interconnection between mitochondrial stress and ER stress. *Cell Death Differ.* 18:769–782. http://dx.doi.org/10.1038/cdd.2010.142

Brand, M.D. 1997. Regulation analysis of energy metabolism. *J. Exp. Biol.* 200:193–202.

Brand, A.H., and N. Perrimon. 1993. Targeted gene expression as a means of altering cell fates and generating dominant phenotypes. *Development.* 118:401–415.

Burman, J.L., S. Yu, A.C. Poole, R.B. Decal, and L. Pallanck. 2012. Analysis of neural subtypes reveals selective mitochondrial dysfunction in dopaminergic neurons from parkin mutants. *Proc. Natl. Acad. Sci. USA.* 109:10438–10443. http://dx.doi.org/10.1073/pnas.1120688109

Cagin, U., O.F. Duncan, A.P. Gatt, M.S. Dionne, S.T. Sweeney, and J.M. Bateman. 2015. Mitochondrial retrograde signaling regulates neuronal function. *Proc. Natl. Acad. Sci. USA.* 112:E6000–E6009. (published erratum appears in *Proc. Natl. Acad. Sci. USA.* 2015. 112:E7032) http://dx.doi.org/10.1073/pnas.1505036112

Celardo, I., A.C. Costa, S. Lehmann, C. Jones, N. Wood, N.E. Mencacci, G.R. Mallucci, S.H.Y. Loh, and L.M. Martins. 2016. Mitofusin-mediated ER stress triggers neurodegeneration in pink1/parkin models of Parkinson's disease. *Cell Death Dis.* 7:e2271. http://dx.doi.org/10.1038/cddis.2016.173

Chen, C.C., J.K. Wu, H.W. Lin, T.P. Pai, T.F. Fu, C.L. Wu, T. Tully, and A.S. Chiang. 2012. Visualizing long-term memory formation in two neurons of the *Drosophila* brain. *Science.* 335:678–685. http://dx.doi.org/10.1126/science.1212735

Chen, H., J.M. McCaffery, and D.C. Chan. 2007. Mitochondrial fusion protects against neurodegeneration in the cerebellum. *Cell.* 130:548–562. http://dx.doi.org/10.1016/j.cell.2007.06.026

Cheng, A., R. Wan, J.-L. Yang, N. Kamimura, T.G. Son, X. Ouyang, Y. Luo, E. Okun, and M.P. Mattson. 2012. Involvement of PGC-1α in the formation and maintenance of neuronal dendritic spines. *Nat. Commun.* 3:1250. http://dx.doi.org/10.1038/ncomms2238

Cheng, H.-C., C.M. Ulane, and R.E. Burke. 2010. Clinical progression in Parkinson disease and the neurobiology of axons. *Ann. Neurol.* 67:715–725. http://dx.doi.org/10.1002/ana.21995

Chihara, T., D. Luginbuhl, and L. Luo. 2007. Cytoplasmic and mitochondrial protein translation in axonal and dendritic terminal arborization. *Nat. Neurosci.* 10:828–837. http://dx.doi.org/10.1038/nn1910

Cichon, J., C. Sun, B. Chen, M. Jiang, X.A. Chen, Y. Sun, Y. Wang, and G. Chen. 2012. Cofilin aggregation blocks intracellular trafficking and induces synaptic loss in hippocampal neurons. *J. Biol. Chem.* 287:3919–3929. http://dx.doi.org/10.1074/jbc.M111.301911

Connolly, N.M.C., H. Düssmann, U. Anilkumar, H.J. Huber, and J.H.M. Prehn. 2014. Single-cell imaging of bioenergetic responses to neuronal excitotoxicity and oxygen and glucose deprivation. *J. Neurosci.* 34:10192–10205. http://dx.doi.org/10.1523/JNEUROSCI.3127-13.2014

Dickey, A.S., and S. Strack. 2011. PKA/AKAP1 and PP2A/Bβ2 regulate neuronal morphogenesis via Drp1 phosphorylation and mitochondrial bioenergetics. *J. Neurosci.* 31:15716–15726. http://dx.doi.org/10.1523/JNEUROSCI.3159-11.2011

DiMauro, S., and E.A. Schon. 2008. Mitochondrial disorders in the nervous system. *Annu. Rev. Neurosci.* 31:91–123. http://dx.doi.org/10.1146/annurev.neuro.30.051606.094302

Dubinsky, J.M. 2009. Heterogeneity of nervous system mitochondria: Location, location, location! *Exp. Neurol.* 218:293–307. http://dx.doi.org/10.1016/j.expneurol.2009.05.020

Echalier, G. 1997. 1 - Composition of the body fluid of drosophila and the design of culture media for *Drosophila* cells. *In Drosophila* Cells in Culture. Academic Press, New York. 1–67. http://dx.doi.org/10.1016/B978-012229460-0/50002-6

Engl, E., and D. Attwell. 2015. Non-signalling energy use in the brain. *J. Physiol.* 593:3417–3429. http://dx.doi.org/10.1113/jphysiol.2014.282517

Engl, E., R. Jolivet, C.N. Hall, and D. Attwell. 2016. Non-signalling energy use in the developing rat brain. *J. Cereb. Blood Flow Metab.*:0271678X16648710.

Erecińska, M., and I.A. Silver. 1989. ATP and brain function. *J. Cereb. Blood Flow Metab.* 9:2–19. http://dx.doi.org/10.1038/jcbfm.1989.2

Evstafieva, A.G., A.A. Garaeva, A.A. Khutornenko, A.V. Klepikova, M.D. Logacheva, A.A. Penin, G.E. Novakovsky, I.E. Kovaleva, and P.M. Chumakov. 2014. A sustained deficiency of mitochondrial respiratory complex III induces an apoptotic cell death through the p53-mediated inhibition of pro-survival activities of the activating transcription factor 4. *Cell Death Dis.* 5:e1511. http://dx.doi.org/10.1038/cddis.2014.469

Fukumitsu, K., K. Fujishima, A. Yoshimura, Y.K. Wu, J. Heuser, and M. Kengaku. 2015. Synergistic action of dendritic mitochondria and creatine kinase maintains ATP homeostasis and actin dynamics in growing neuronal dendrites. *J. Neurosci.* 35:5707–5723. http://dx.doi.org/10.1523/JNEUROSCI.4115-14.2015

Gao, F.B., J.E. Brenman, L.Y. Jan, and Y.N. Jan. 1999. Genes regulating dendritic outgrowth, branching, and routing in *Drosophila*. *Genes Dev.* 13:2549–2561. http://dx.doi.org/10.1101/gad.13.19.2549

Greaves, L.C., A.K. Reeve, R.W. Taylor, and D.M. Turnbull. 2012. Mitochondrial DNA and disease. *J. Pathol.* 226:274–286. http://dx.doi.org/10.1002/path.3028

Griparic, L., N.N. van der Wel, I.J. Orozco, P.J. Peters, and A.M. van der Bliek. 2004. Loss of the intermembrane space protein Mgm1/OPA1 induces swelling and localized constrictions along the lengths of mitochondria. *J. Biol. Chem.* 279:18792–18798. http://dx.doi.org/10.1074/jbc.M400920200

Grueber, W.B., L.Y. Jan, and Y.N. Jan. 2002. Tiling of the *Drosophila* epidermis by multidendritic sensory neurons. *Development.* 129:2867–2878.

Grueber, W.B., L.Y. Jan, and Y.N. Jan. 2003. Different levels of the homeodomain protein cut regulate distinct dendrite branching patterns of *Drosophila* multidendritic neurons. *Cell.* 112:805–818. http://dx.doi.org/10.1016/S0092-8674(03)00160-0

Haddad, D., and K. Nakamura. 2015. Understanding the susceptibility of dopamine neurons to mitochondrial stressors in Parkinson's disease. *FEBS Lett.* 589(24PartA, 24 Pt A):3702–3713. http://dx.doi.org/10.1016/j.febslet.2015.10.021

Haelterman, N.A., W.H. Yoon, H. Sandoval, M. Jaiswal, J.M. Shulman, and H.J. Bellen. 2014. A mitocentric view of Parkinson's disease. *Annu. Rev. Neurosci.* 37:137–159. http://dx.doi.org/10.1146/annurev-neuro-071013-014317

Han, C., Y. Song, H. Xiao, D. Wang, N.C. Franc, L.Y. Jan, and Y.N. Jan. 2014. Epidermal cells are the primary phagocytes in the fragmentation and clearance of degenerating dendrites in *Drosophila*. *Neuron.* 81:544–560. http://dx.doi.org/10.1016/j.neuron.2013.11.021

Hardie, D.G., F.A. Ross, and S.A. Hawley. 2012. AMPK: A nutrient and energy sensor that maintains energy homeostasis. *Nat. Rev. Mol. Cell Biol.* 13:251–262. http://dx.doi.org/10.1038/nrm3311

Hasel, P., S. Mckay, J. Qiu, and G.E. Hardingham. 2015. Selective dendritic susceptibility to bioenergetic, excitotoxic and redox perturbations in cortical neurons. *Biochim. Biophys. Acta.* 1853:2066–2076. http://dx.doi.org/10.1016/j.bbamcr.2014.12.021

Hay, B.A., T. Wolff, and G.M. Rubin. 1994. Expression of baculovirus P35 prevents cell death in *Drosophila*. *Development.* 120:2121–2129.

Hofmeyr, J.-H.S. 2008. The harmony of the cell: The regulatory design of cellular processes. *Essays Biochem.* 45:57–66. http://dx.doi.org/10.1042/bse0450057

Hoozemans, J.J.M., E.S. van Haastert, P. Eikelenboom, R.A.I. de Vos, J.M. Rozemuller, and W. Scheper. 2007. Activation of the unfolded protein response in Parkinson's disease. *Biochem. Biophys. Res. Commun.* 354:707–711. http://dx.doi.org/10.1016/j.bbrc.2007.01.043

Howarth, C., P. Gleeson, and D. Attwell. 2012. Updated energy budgets for neural computation in the neocortex and cerebellum. *J. Cereb. Blood Flow Metab.* 32:1222–1232. http://dx.doi.org/10.1038/jcbfm.2012.35

Huang, H., X. Zhang, S. Li, N. Liu, W. Lian, E. McDowell, P. Zhou, C. Zhao, H. Guo, C. Zhang, et al. 2010. Physiological levels of ATP negatively regulate proteasome function. *Cell Res.* 20:1372–1385. http://dx.doi.org/10.1038/cr.2010.123

Im, S.H., K. Takle, J. Jo, D.T. Babcock, Z. Ma, Y. Xiang, and M.J. Galko. 2015. Tachykinin acts upstream of autocrine Hedgehog signaling during nociceptive sensitization in *Drosophila*. *eLife.* 4:e10735. http://dx.doi.org/10.7554/eLife.10735

Imamura, H., K.P.H. Nhat, H. Togawa, K. Saito, R. Iino, Y. Kato-Yamada, T. Nagai, and H. Noji. 2009. Visualization of ATP levels inside single living cells with fluorescence resonance energy transfer-based genetically encoded indicators. *Proc. Natl. Acad. Sci. USA.* 106:15651–15656. http://dx.doi.org/10.1073/pnas.0904764106

Itoh, K., K. Nakamura, M. Iijima, and H. Sesaki. 2013. Mitochondrial dynamics in neurodegeneration. *Trends Cell Biol.* 23:64–71. http://dx.doi.org/10.1016/j.tcb.2012.10.006

Itoh, Y., T. Abe, R. Takaoka, and N. Tanahashi. 2004. Fluorometric determination of glucose utilization in neurons in vitro and in vivo. *J. Cereb. Blood Flow Metab.* 24:993–1003. http://dx.doi.org/10.1097/01.WCB.0000127661.07591.DE

Iyer, E.P.R., S.C. Iyer, L. Sullivan, D. Wang, R. Meduri, L.L. Graybeal, and D.N. Cox. 2013. Functional genomic analyses of two morphologically distinct classes of *Drosophila* sensory neurons: Post-mitotic roles of transcription factors in dendritic patterning. *PLoS One.* 8:e72434. http://dx.doi.org/10.1371/journal.pone.0072434

Jan, Y.N., and L.Y. Jan. 2010. Branching out: Mechanisms of dendritic arborization. *Nat. Rev. Neurosci.* 11:316–328. http://dx.doi.org/10.1038/nrn2836

Janssen, G.M.C., P. Schwertman, T.A.T. Wanga, R.S.J. Tafrechi, P.J. van den Broek, and A.K. Raap. 2009. Transient and constitutive repression of cytoplasmic translation signaling in cells with mtDNA mutation. *Cell. Mol. Life Sci.* 66:721–730. http://dx.doi.org/10.1007/s00018-009-8687-4

Johnson, E.C., N. Kazgan, C.A. Bretz, L.J. Forsberg, C.E. Hector, R.J. Worthen, R. Onyenwoke, and J.E. Brenman. 2010. Altered metabolism and persistent starvation behaviors caused by reduced AMPK function in *Drosophila*. *PLoS One.* 5:e12799. http://dx.doi.org/10.1371/journal.pone.0012799

Kim, H.-J., A.R. Raphael, E.S. LaDow, L. McGurk, R.A. Weber, J.Q. Trojanowski, V.M.-Y. Lee, S. Finkbeiner, A.D. Gitler, and N.M. Bonini. 2014. Therapeutic modulation of eIF2α phosphorylation rescues TDP-43 toxicity in amyotrophic lateral sclerosis disease models. *Nat. Genet.* 46:152–160. http://dx.doi.org/10.1038/ng.2853

Koike, T., Y. Yang, K. Suzuki, and X. Zheng. 2008. Axon and dendrite degeneration: Its mechanisms and protective experimental paradigms. *Neurochem. Int.* 52:751–760. http://dx.doi.org/10.1016/j.neuint.2007.09.007

Koike-Kumagai, M., K. Yasunaga, R. Morikawa, T. Kanamori, and K. Emoto. 2009. The target of rapamycin complex 2 controls dendritic tiling of *Drosophila* sensory neurons through the Tricornered kinase signalling pathway. *EMBO J.* 28:3879–3892. http://dx.doi.org/10.1038/emboj.2009.312

Koopman, W.J.H., F. Distelmaier, J.A. Smeitink, and P.H. Willems. 2012. OXP HOS mutations and neurodegeneration. *EMBO J.* 32:9–29. http://dx.doi.org/10.1038/emboj.2012.300

Leung, K.-M., and C.E. Holt. 2008. Live visualization of protein synthesis in axonal growth cones by microinjection of photoconvertible Kaede into *Xenopus* embryos. *Nat. Protoc.* 3:1318–1327. http://dx.doi.org/10.1038/nprot.2008.113

Li, J., J.J. Wang, and S.X. Zhang. 2011. Preconditioning with endoplasmic reticulum stress mitigates retinal endothelial inflammation via activation of X-box binding protein 1. *J. Biol. Chem.* 286:4912–4921. http://dx.doi.org/10.1074/jbc.M110.199729

Liu, S., and B. Lu. 2010. Reduction of protein translation and activation of autophagy protect against PINK1 pathogenesis in *Drosophila melanogaster*. *PLoS Genet.* 6:e1001237. http://dx.doi.org/10.1371/journal.pgen.1001237

Liu, Z., R. Steward, and L. Luo. 2000. *Drosophila* Lis1 is required for neuroblast proliferation, dendritic elaboration and axonal transport. *Nat. Cell Biol.* 2:776–783. http://dx.doi.org/10.1038/35041011

Lu, B., S. Gehrke, and Z. Wu. 2014. RNA metabolism in the pathogenesis of Parkinson's disease. *Brain Res.* 1584:105–115. http://dx.doi.org/10.1016/j.brainres.2014.03.003

Macleod, G.T., M. Hegström-Wojtowicz, M.P. Charlton, and H.L. Atwood. 2002. Fast calcium signals in *Drosophila* motor neuron terminals. *J. Neurophysiol.* 88:2659–2663. http://dx.doi.org/10.1152/jn.00515.2002

Maltecca, F., E. Baseggio, F. Consolato, D. Mazza, P. Podini, S.M. Young Jr., I. Drago, B.A. Bahr, A. Puliti, F. Codazzi, et al. 2015. Purkinje neuron Ca2+ influx reduction rescues ataxia in SCA28 model. *J. Clin. Invest.* 125:263–274. http://dx.doi.org/10.1172/JCI74770

Malthankar-Phatak, G.H., A.B. Patel, Y. Xia, S. Hong, G.M.I. Chowdhury, K.L. Behar, I.A. Orina, and J.C.K. Lai. 2008. Effects of continuous hypoxia on energy metabolism in cultured cerebro-cortical neurons. *Brain Res.* 1229:147–154. http://dx.doi.org/10.1016/j.brainres.2008.06.074

Malzer, E., M.L. Daly, A. Moloney, T.J. Sendall, S.E. Thomas, E. Ryder, H.D. Ryoo, D.C. Crowther, D.A. Lomas, and S.J. Marciniak. 2010. Impaired tissue growth is mediated by checkpoint kinase 1 (CHK1) in the integrated stress response. *J. Cell Sci.* 123:2892–2900. http://dx.doi.org/10.1242/jcs.070078

Malzer, E., M. Szajewska-Skuta, L.E. Dalton, S.E. Thomas, N. Hu, H. Skaer, D.A. Lomas, D.C. Crowther, and S.J. Marciniak. 2013. Coordinate regulation of eIF2α phosphorylation by PPP1R15 and GCN2 is required during *Drosophila* development. *J. Cell Sci.* 126:1406–1415. http://dx.doi.org/10.1242/jcs.117614

Mandal, S., P. Guptan, E. Owusu-Ansah, and U. Banerjee. 2005. Mitochondrial regulation of cell cycle progression during development as revealed by the tenured mutation in *Drosophila*. *Dev. Cell.* 9:843–854. http://dx.doi.org/10.1016/j.devcel.2005.11.006

Michel, S., M. Canonne, T. Arnould, and P. Renard. 2015. Inhibition of mitochondrial genome expression triggers the activation of CHOP-10 by a cell signaling dependent on the integrated stress response but not the mitochondrial unfolded protein response. *Mitochondrion.* 21:58–68. http://dx.doi.org/10.1016/j.mito.2015.01.005

Misko, A.L., Y. Sasaki, E. Tuck, J. Milbrandt, and R.H. Baloh. 2012. Mitofusin2 mutations disrupt axonal mitochondrial positioning and promote axon degeneration. *J. Neurosci.* 32:4145–4155. http://dx.doi.org/10.1523/JNEUROSCI.6338-11.2012

Mizuno, H., T.K. Mal, K.I. Tong, R. Ando, T. Furuta, M. Ikura, and A. Miyawaki. 2003. Photo-induced peptide cleavage in the green-to-red conversion of a fluorescent protein. *Mol. Cell.* 12:1051–1058. http://dx.doi.org/10.1016/S1097-2765(03)00393-9

Monaghan, R.M., and A.J. Whitmarsh. 2015. Mitochondrial proteins moonlighting in the nucleus. *Trends Biochem. Sci.* 40:728–735. http://dx.doi.org/10.1016/j.tibs.2015.10.003

Morais, V.A., P. Verstreken, A. Roethig, J. Smet, A. Snellinx, M. Vanbrabant, D. Haddad, C. Frezza, W. Mandemakers, D. Vogt-Weisenhorn, et al. 2009. Parkinson's disease mutations in PINK1 result in decreased Complex I activity and deficient synaptic function. *EMBO Mol. Med.* 1:99–111. http://dx.doi.org/10.1002/emmm.200900006

Mori, K. 2009. Signalling pathways in the unfolded protein response: Development from yeast to mammals. *J. Biochem.* 146:743–750. http://dx.doi.org/10.1093/jb/mvp166

Mutez, E., A. Nkiliza, K. Belarbi, A. de Broucker, C. Vanbesien-Mailliot, S. Bleuse, A. Duflot, T. Comptdaer, P. Semaille, R. Blervaque, et al. 2014. Involvement of the immune system, endocytosis and EIF2 signaling in both genetically determined and sporadic forms of Parkinson's disease. *Neurobiol. Dis.* 63:165–170. http://dx.doi.org/10.1016/j.nbd.2013.11.007

Naidoo, N., M. Ferber, M. Master, Y. Zhu, and A.I. Pack. 2008. Aging impairs the unfolded protein response to sleep deprivation and leads to proapoptotic signaling. *J. Neurosci.* 28:6539–6548. http://dx.doi.org/10.1523/JNEUROSCI.5685-07.2008

Naon, D., and L. Scorrano. 2014. At the right distance: ER-mitochondria juxtaposition in cell life and death. *Biochim. Biophys. Acta.* 1843:2184–2194. http://dx.doi.org/10.1016/j.bbamcr.2014.05.011

Niehues, S., J. Bussmann, G. Steffes, I. Erdmann, C. Köhrer, L. Sun, M. Wagner, K. Schäfer, G. Wang, S.N. Koerdt, et al. 2015. Impaired protein translation in *Drosophila* models for Charcot-Marie-Tooth neuropathy caused by mutant tRNA synthetases. *Nat. Commun.* 6:7520. http://dx.doi.org/10.1038/ncomms8520

Niven, J.E., and S.B. Laughlin. 2008. Energy limitation as a selective pressure on the evolution of sensory systems. *J. Exp. Biol.* 211:1792–1804. http://dx.doi.org/10.1242/jeb.017574

Nunnari, J., and A. Suomalainen. 2012. Mitochondria: In sickness and in health. *Cell.* 148:1145–1159. http://dx.doi.org/10.1016/j.cell.2012.02.035

Olichon, A., T. Landes, L. Arnauné-Pelloquin, L.J. Emorine, V. Mils, A. Guichet, C. Delettre, C. Hamel, P. Amati-Bonneau, D. Bonneau, et al. 2007. Effects of OPA1 mutations on mitochondrial morphology and apoptosis: Relevance to ADOA pathogenesis. *J. Cell. Physiol.* 211:423–430. http://dx.doi.org/10.1002/jcp.20950

Ollmann, M., L.M. Young, C.J. Di Como, F. Karim, M. Belvin, S. Robertson, K. Whittaker, M. Demsky, W.W. Fisher, A. Buchman, et al. 2000. *Drosophila* p53 is a structural and functional homolog of the tumor suppressor p53. *Cell.* 101:91–101. http://dx.doi.org/10.1016/S0092-8674(00)80626-1

Oruganty-Das, A., T. Ng, T. Udagawa, E.L.K. Goh, and J.D. Richter. 2012. Translational control of mitochondrial energy production mediates neuron morphogenesis. *Cell Metab.* 16:789–800. http://dx.doi.org/10.1016/j.cmet.2012.11.002

Owusu-Ansah, E., A. Yavari, S. Mandal, and U. Banerjee. 2008. Distinct mitochondrial retrograde signals control the G1-S cell cycle checkpoint. *Nat. Genet.* 40:356–361. http://dx.doi.org/10.1038/ng.2007.50

Pacelli, C., N. Giguère, M.-J. Bourque, M. Lévesque, R.S. Slack, and L.-É. Trudeau. 2015. Elevated mitochondrial bioenergetics and axonal arborization size are key contributors to the vulnerability of dopamine neurons. *Curr. Biol.* 25:2349–2360. http://dx.doi.org/10.1016/j.cub.2015.07.050

Pathak, D., A. Berthet, and K. Nakamura. 2013. Energy failure: Does it contribute to neurodegeneration? *Ann. Neurol.* 74:506–516. http://dx.doi.org/10.1002/ana.24014

Pathak, D., L.Y. Shields, B.A. Mendelsohn, D. Haddad, W. Lin, A.A. Gerencser, H. Kim, M.D. Brand, R.H. Edwards, and K. Nakamura. 2015. The role of mitochondrially derived ATP in synaptic vesicle recycling. *J. Biol. Chem.* 290:22325–22336. http://dx.doi.org/10.1074/jbc.M115.656405

Patt, S., H.J. Gertz, L. Gerhard, and J. Cervós-Navarro. 1991. Pathological changes in dendrites of substantia nigra neurons in Parkinson's disease: A Golgi study. *Histol. Histopathol.* 6:373–380.

Pomar, N., J.J. Berlanga, S. Campuzano, G. Hernández, M. Elías, and C. de Haro. 2003. Functional characterization of *Drosophila* melanogaster PERK eukaryotic initiation factor 2alpha (eIF2alpha) kinase. *Eur. J. Biochem.* 270:293–306. http://dx.doi.org/10.1046/j.1432-1033.2003.03383.x

Price, J.C., S. Guan, A. Burlingame, S.B. Prusiner, and S. Ghaemmaghami. 2010. Analysis of proteome dynamics in the mouse brain. *Proc. Natl. Acad. Sci. USA.* 107:14508–14513. (published erratum appears in *Proc. Natl. Acad. Sci. USA*. 2014. 111:3645) http://dx.doi.org/10.1073/pnas.1006551107

Purdon, A.D., and S.I. Rapoport. 2007. Energy consumption by phospholipid metabolism in mammalian brain. In Handbook of Neurochemistry and Molecular Neurobiology. Springer US. Boston, MA. 401–427. http://dx.doi.org/10.1007/978-0-387-30411-3_15

Raimundo, N. 2014. Mitochondrial pathology: Stress signals from the energy factory. *Trends Mol. Med.* 20:282–292. http://dx.doi.org/10.1016/j.molmed.2014.01.005

Ramachandran, P., and V. Budnik. 2010. Preparation of late *Drosophil*a embryonic fillets. *Cold Spring Harb. Protoc*. 2010:pdb.prot5498. http://dx.doi.org/10.1101/pdb.prot5498

Rangaraju, V., N. Calloway, and T.A. Ryan. 2014. Activity-driven local ATP synthesis is required for synaptic function. *Cell.* 156:825–835. http://dx.doi.org/10.1016/j.cell.2013.12.042

Remmen, H., W.F. Ward, and R.V. Sabia. 2011. Gene expression and protein degradation. *Compr. Physiol.* 28:171–234. http://dx.doi.org/10.1002/cphy.cp110109

Ren, M., C.K.L. Phoon, and M. Schlame. 2014. Metabolism and function of mitochondrial cardiolipin. *Prog. Lipid Res.* 55:1–16. http://dx.doi.org/10.1016/j.plipres.2014.04.001

Requejo-Aguilar, R., I. Lopez-Fabuel, E. Fernández, L.M. Martins, A. Almeida, and J.P. Bolaños. 2014. PINK1 deficiency sustains cell proliferation by reprogramming glucose metabolism through HIF1. *Nat. Commun.* 5:4514. http://dx.doi.org/10.1038/ncomms5514

Rolfe, D.F., and G.C. Brown. 1997. Cellular energy utilization and molecular origin of standard metabolic rate in mammals. *Physiol. Rev.* 77:731–758.

Rossignol, R., B. Faustin, C. Rocher, M. Malgat, J.-P. Mazat, and T. Letellier. 2003. Mitochondrial threshold effects. *Biochem. J.* 370:751–762. http://dx.doi.org/10.1042/bj20021594

Rutkowski, D.T., and R.S. Hegde. 2010. Regulation of basal cellular physiology by the homeostatic unfolded protein response. *J. Cell Biol.* 189:783–794. http://dx.doi.org/10.1083/jcb.201003138

Ryoo, H.D., P.M. Domingos, M.-J. Kang, and H. Steller. 2007. Unfolded protein response in a *Drosophila* model for retinal degeneration. *EMBO J.* 26:242–252. http://dx.doi.org/10.1038/sj.emboj.7601477

Ryu, E.J., J.M. Angelastro, and L.A. Greene. 2005. Analysis of gene expression changes in a cellular model of Parkinson disease. *Neurobiol. Dis.* 18:54–74. http://dx.doi.org/10.1016/j.nbd.2004.08.016

San Martín, A., T. Sotelo-Hitschfeld, R. Lerchundi, I. Fernández-Moncada, S. Ceballo, R. Valdebenito, F. Baeza-Lehnert, K. Alegría, Y. Contreras-Baeza, P. Garrido-Gerter, et al. 2014. Single-cell imaging tools for brain energy metabolism: A review. *Neurophotonics.* 1:011004. http://dx.doi.org/10.1117/1.NPh.1.1.011004

Scheper, W., and J.J.M. Hoozemans. 2015. The unfolded protein response in neurodegenerative diseases: A neuropathological perspective. *Acta Neuropathol.* 130:315–331. http://dx.doi.org/10.1007/s00401-015-1462-8

Scheper, G.C., M.S. van der Knaap, and C.G. Proud. 2007. Translation matters: Protein synthesis defects in inherited disease. *Nat. Rev. Genet.* 8:711–723. http://dx.doi.org/10.1038/nrg2142

Schirmeier, S., T. Matzat, and C. Klämbt. 2015. Axon ensheathment and metabolic supply by glial cells in *Drosophila*. *Brain Res.* 1641:122–129. http://dx.doi.org/10.1016/j.brainres.2015.09.003

Schneider, C.A., W.S. Rasband, and K.W. Eliceiri. 2012. NIH Image to ImageJ: 25 years of image analysis. *Nat. Methods.* 9:671–675. http://dx.doi.org/10.1038/nmeth.2089

Sekine, S.U., S. Haraguchi, K. Chao, T. Kato, L. Luo, M. Miura, and T. Chihara. 2013. Meigo governs dendrite targeting specificity by modulating ephrin level and N-glycosylation. *Nat. Neurosci.* 16:683–691. http://dx.doi.org/10.1038/nn.3389

Senft, D., and Z.A. Ronai. 2015. UPR, autophagy, and mitochondria crosstalk underlies the ER stress response. *Trends Biochem. Sci.* 40:141–148. http://dx.doi.org/10.1016/j.tibs.2015.01.002

Shepherd, D., and S.A. Smith. 1996. Central projections of persistent larval sensory neurons prefigure adult sensory pathways in the CNS of *Drosophila. Development.* 122:2375–2384.

Shields, L.Y., H. Kim, L. Zhu, D. Haddad, A. Berthet, D. Pathak, M. Lam, R. Ponnusamy, L.G. Diaz-Ramirez, T.M. Gill, et al. 2015. Dynamin-related protein 1 is required for normal mitochondrial bioenergetic and synaptic function in CA1 hippocampal neurons. *Cell Death Dis.* 6:e1725. http://dx.doi.org/10.1038/cddis.2015.94

Shimono, K., K. Fujishima, T. Nomura, M. Ohashi, T. Usui, M. Kengaku, A. Toyoda, and T. Uemura. 2014. An evolutionarily conserved protein CHORD regulates scaling of dendritic arbors with body size. *Sci. Rep.* 4:4415. http://dx.doi.org/10.1038/srep04415

Song, W., M. Onishi, L.Y. Jan, and Y.N. Jan. 2007. Peripheral multidendritic sensory neurons are necessary for rhythmic locomotion behavior in *Drosophila* larvae. *Proc. Natl. Acad. Sci. USA.* 104:5199–5204. http://dx.doi.org/10.1073/pnas.0700895104

Storey, K.B., and J.M. Storey. 2007. Tribute to P. L. Lutz: Putting life on 'pause'—molecular regulation of hypometabolism. *J. Exp. Biol.* 210:1700–1714. http://dx.doi.org/10.1242/jeb.02716

Strang, R., and E.M. Clement. 1980. The relative importance of glucose and trehalose in the nutrition of the nervous system of the locust *Schistocerca americana gregaria*. *Insect Biochem.* 10:155–161. http://dx.doi.org/10.1016/0020-1790(80)90067-0

Sugimura, K., M. Yamamoto, R. Niwa, D. Satoh, S. Goto, M. Taniguchi, S. Hayashi, and T. Uemura. 2003. Distinct developmental modes and lesion-induced reactions of dendrites of two classes of *Drosophila* sensory neurons. *J. Neurosci.* 23:3752–3760.

Sugiyama, S., S. Moritoh, Y. Furukawa, T. Mizuno, Y.-M. Lim, L. Tsuda, and Y. Nishida. 2007. Involvement of the mitochondrial protein translocator component tim50 in growth, cell proliferation and the modulation of respiration in *Drosophila*. *Genetics.* 176:927–936. http://dx.doi.org/10.1534/genetics.107.072074

Sun, X., J. Liu, J.F. Crary, C. Malagelada, D. Sulzer, L.A. Greene, and O.A. Levy. 2013. ATF4 protects against neuronal death in cellular Parkinson's disease models by maintaining levels of parkin. *J. Neurosci.* 33:2398–2407. http://dx.doi.org/10.1523/JNEUROSCI.2292-12.2013

Surin, A.M., S. Khiroug, L.R. Gorbacheva, B.I. Khodorov, V.G. Pinelis, and L. Khiroug. 2013. Comparative analysis of cytosolic and mitochondrial ATP synthesis in embryonic and postnatal hippocampal neuronal cultures. *Front. Mol. Neurosci.* 5:102. http://dx.doi.org/10.3389/fnmol.2012.00102

Sutton, M.A., and E.M. Schuman. 2006. Dendritic protein synthesis, synaptic plasticity, and memory. *Cell.* 127:49–58. http://dx.doi.org/10.1016/j.cell.2006.09.014

Tain, L.S., H. Mortiboys, R.N. Tao, E. Ziviani, O. Bandmann, and A.J. Whitworth. 2009. Rapamycin activation of 4E-BP prevents parkinsonian dopaminergic neuron loss. *Nat. Neurosci.* 12:1129–1135. http://dx.doi.org/10.1038/nn.2372

Tamura, Y., T. Endo, M. Iijima, and H. Sesaki. 2009. Ups1p and Ups2p antagonistically regulate cardiolipin metabolism in mitochondria. *J. Cell Biol.* 185:1029–1045. http://dx.doi.org/10.1083/jcb.200812018

Tanaka, T., K. Nagashima, N. Inagaki, H. Kioka, S. Takashima, H. Fukuoka, H. Noji, A. Kakizuka, and H. Imamura. 2014. Glucose-stimulated single pancreatic islets sustain increased cytosolic ATP levels during initial Ca2+ influx and subsequent Ca2+ oscillations. *J. Biol. Chem.* 289:2205–2216. http://dx.doi.org/10.1074/jbc.M113.499111

Tatsuta, T., M. Scharwey, and T. Langer. 2014. Mitochondrial lipid trafficking. *Trends Cell Biol.* 24:44–52. http://dx.doi.org/10.1016/j.tcb.2013.07.011

Taymans, J.-M., A. Nkiliza, and M.-C. Chartier-Harlin. 2015. Deregulation of protein translation control, a potential game-changing hypothesis for Parkinson's disease pathogenesis. *Trends Mol. Med.* 21:466–472. http://dx.doi.org/10.1016/j.molmed.2015.05.004

Tian, X., M. Zhu, L. Li, and C. Wu. 2013. Identifying protein-protein interaction in *Drosophila* adult heads by tandem affinity purification (TAP). *J. Vis. Exp.* 82:50968. http://dx.doi.org/10.3791/50968

Toloe, J., R. Mollajew, S. Kügler, and S.L. Mironov. 2014. Metabolic differences in hippocampal 'Rett' neurons revealed by ATP imaging. *Mol. Cell. Neurosci.* 59:47–56. http://dx.doi.org/10.1016/j.mcn.2013.12.008

Tsubouchi, A., T. Tsuyama, M. Fujioka, H. Kohda, K. Okamoto-Furuta, T. Aigaki, and T. Uemura. 2009. Mitochondrial protein Preli-like is required for development of dendritic arbors and prevents their regression in the *Drosophila* sensory nervous system. *Development.* 136:3757–3766. http://dx.doi.org/10.1242/dev.042135

Tsuyama, T., J. Kishikawa, Y.-W. Han, Y. Harada, A. Tsubouchi, H. Noji, A. Kakizuka, K. Yokoyama, T. Uemura, and H. Imamura. 2013. In vivo fluorescent adenosine 5′-triphosphate (ATP) imaging of *Drosophila* melanogaster and *Caenorhabditis elegans* by using a genetically encoded fluorescent ATP biosensor optimized for low temperatures. *Anal. Chem.* 85:7889–7896. http://dx.doi.org/10.1021/ac4015325

Ui-Tei, K., S. Nishihara, M. Sakuma, K. Matsuda, T. Miyake, and Y. Miyata. 1994. Chemical analysis of neurotransmitter candidates in clonal cell lines from *Drosophila* central nervous system. I. ACh and L-dopa. *Neurosci. Lett.* 174:85–88. http://dx.doi.org/10.1016/0304-3940(94)90125-2

Valdés, P., G. Mercado, R.L. Vidal, C. Molina, G. Parsons, F.A. Court, A. Martinez, D. Galleguillos, D. Armentano, B.L. Schneider, and C. Hetz. 2014. Control of dopaminergic neuron survival by the unfolded protein response transcription factor XBP1. *Proc. Natl. Acad. Sci. USA*. 111:6804–6809. http://dx.doi.org/10.1073/pnas.1321845111

Verstreken, P., C.V. Ly, K.J.T. Venken, T.-W. Koh, Y. Zhou, and H.J. Bellen. 2005. Synaptic mitochondria are critical for mobilization of reserve pool vesicles at *Drosophila* neuromuscular junctions. *Neuron.* 47:365–378. http://dx.doi.org/10.1016/j.neuron.2005.06.018

Vincow, E.S., G. Merrihew, R.E. Thomas, N.J. Shulman, R.P. Beyer, M.J. MacCoss, and L.J. Pallanck. 2013. The PINK1-Parkin pathway promotes both mitophagy and selective respiratory chain turnover in vivo. *Proc. Natl. Acad. Sci. USA*. 110:6400–6405. http://dx.doi.org/10.1073/pnas.1221132110

Wallace, D.C., and W. Fan. 2009. The pathophysiology of mitochondrial disease as modeled in the mouse. *Genes Dev.* 23:1714–1736. http://dx.doi.org/10.1101/gad.1784909

Walter, P., and D. Ron. 2011. The unfolded protein response: From stress pathway to homeostatic regulation. *Science.* 334:1081–1086. http://dx.doi.org/10.1126/science.1209038

Wei, X., A.S. Howell, X. Dong, C.A. Taylor, R.C. Cooper, J. Zhang, W. Zou, D.R. Sherwood, K. Shen, and G.W. Davis. 2015. The unfolded protein response is required for dendrite morphogenesis. *eLife.* 4:e06963. http://dx.doi.org/10.7554/eLife.06963

Weisová, P., C.G. Concannon, M. Devocelle, J.H.M. Prehn, and M.W. Ward. 2009. Regulation of glucose transporter 3 surface expression by the AMP-activated protein kinase mediates tolerance to glutamate excitation in neurons. *J. Neurosci.* 29:2997–3008. http://dx.doi.org/10.1523/JNEUROSCI.0354-09.2009

Wek, R.C., H.-Y. Jiang, and T.G. Anthony. 2006. Coping with stress: eIF2 kinases and translational control. *Biochem. Soc. Trans.* 34:7–11. http://dx.doi.org/10.1042/BST0340007

Williams, P.A., J.E. Morgan, and M. Votruba. 2010. Opa1 deficiency in a mouse model of dominant optic atrophy leads to retinal ganglion cell dendropathy. *Brain.* 133:2942–2951. http://dx.doi.org/10.1093/brain/awq218

Wong-Riley, M.T.T. 2012. Bigenomic regulation of cytochrome c oxidase in neurons and the tight coupling between neuronal activity and energy metabolism. *Adv. Exp. Med. Biol.* 748:283–304. http://dx.doi.org/10.1007/978-1-4614-3573-0_12

Wu, J.S., and L. Luo. 2006. A protocol for mosaic analysis with a repressible cell marker (MARCM) in *Drosophila*. *Nat. Protoc.* 1:2583–2589. http://dx.doi.org/10.1038/nprot.2006.320

Xiang, Y., Q. Yuan, N. Vogt, L.L. Looger, L.Y. Jan, and Y.N. Jan. 2010. Light-avoidance-mediating photoreceptors tile the Drosophila larval body wall. *Nature*. 468:921–926. http://dx.doi.org/10.1038/nature09576

Yaginuma, H., S. Kawai, K.V. Tabata, K. Tomiyama, A. Kakizuka, T. Komatsuzaki, H. Noji, and H. Imamura. 2014. Diversity in ATP concentrations in a single bacterial cell population revealed by quantitative single-cell imaging. *Sci. Rep.* 4:6522. http://dx.doi.org/10.1038/srep06522

Yamamoto, M., R. Ueda, K. Takahashi, K. Saigo, and T. Uemura. 2006. Control of axonal sprouting and dendrite branching by the Nrg-Ank complex at the neuron-glia interface. *Curr. Biol.* 16:1678–1683. http://dx.doi.org/10.1016/j.cub.2006.06.061

Yang, J., Z. Wu, N. Renier, D.J. Simon, K. Uryu, D.S. Park, P.A. Greer, C. Tournier, R.J. Davis, and M. Tessier-Lavigne. 2015. Pathological axonal death through a MAPK cascade that triggers a local energy deficit. *Cell.* 160:161–176. http://dx.doi.org/10.1016/j.cell.2014.11.053

Ying, W. 2008. NAD+/NADH and NADP+/NADPH in cellular functions and cell death: Regulation and biological consequences. *Antioxid. Redox Signal.* 10:179–206. http://dx.doi.org/10.1089/ars.2007.1672

Ylikallio, E., H. Tyynismaa, H. Tsutsui, T. Ide, and A. Suomalainen. 2010. High mitochondrial DNA copy number has detrimental effects in mice. *Hum. Mol. Genet.* 19:2695–2705. http://dx.doi.org/10.1093/hmg/ddq163

Zhang, X., E. Szabo, M. Michalak, and M. Opas. 2007. Endoplasmic reticulum stress during the embryonic development of the central nervous system in the mouse. *Int. J. Dev. Neurosci.* 25:455–463. http://dx.doi.org/10.1016/j.ijdevneu.2007.08.007

Zhou, L., A. Chomyn, G. Attardi, and C.A. Miller. 1997. Myoclonic epilepsy and ragged red fibers (MERRF) syndrome: Selective vulnerability of CNS neurons does not correlate with the level of mitochondrial tRNAlys mutation in individual neuronal isolates. *J. Neurosci.* 17:7746–7753.